# U-Pb Zircon Ages of the Knight Peak Outflow Sheet and Lava Sequence, Mogollon-Datil Volcanic Field, New Mexico, USA: Implications for Magmatism and Extension in the Southeastern Basin and Range Province

Jeffrey M. Amato<sup>1</sup>, Vanessa M. Swenton<sup>1,2</sup>, and Jaime Toro<sup>3</sup>

- <sup>1</sup> Department of Geological Sciences, New Mexico State University, Las Cruces, NM 88003; amato@nmsu.edu
- <sup>2</sup> Now at: Oregon Department of Geology and Mineral Industries, Portland, OR 97232; vanessa.swenton@dogami.oregon.gov
- <sup>3</sup> Department of Geology and Geography, West Virginia University, 330 Brooks Hall, P.O. Box 6300, Morgantown, WV 26506; jtoro@wvu.edu

https://doi.org/10.58799/NMG-v46n3.31

#### **Abstract**

The volcanic rocks of the Knight Peak region of the southern Mogollon-Datil volcanic field (MDVF) consist of a stratigraphic sequence of ignimbrite outflow sheets and lava flows. These rocks were deposited unconformably on a ca. 1.46 Ga granite. The total thickness is more than 1100 m. We used U-Pb zircon geochronology to date four of the previously undated volcanic units and a rhyolite dike that is part of a swarm that intruded the Proterozoic granite. The rhyolite dike had an age of 58.6 ± 0.6 Ma (all new ages are weighted mean  $^{238}$ U/ $^{206}$ Pb dates with errors reported at the  $2\sigma$  level). This dike is part of a swarm likely related to ore-bearing intrusions, such as the Tyrone pluton, that were emplaced during the Laramide orogeny. The dike swarm orientations are consistent with northeast-southwest Laramide shortening. The oldest volcanic rock in the Knight Peak sequence that we dated is the 36.2 ± 0.4 Ma JPB Mountain trachyte. This lava flow is among the oldest eruptions in the western MDVF and has no currently known correlative units. The next unit consists of a series of thick rhyolite ignimbrites, collectively mapped as the C-Bar Canyon tuff and tuff breccia and originally mapped as a tuff breccia, with a total thickness of 400 m in the study area. This unit forms the cliffs of the summit of Knight Peak. The tuff is crystal-poor and did not yield sanidine. The U-Pb ages of samples from the tuff breccia and the rhyolite tuff were 35.2 ± 0.4 and 35.2 ± 0.6 Ma, respectively. Given the overall thickness and presence of coarse lithic fragments in the tuff, this unit was likely sourced from near Knight Peak, but the overall stratigraphic continuity makes it unlikely to be intracaldera fill. The next-youngest tuff was originally mapped as the Kneeling Nun Tuff (Hedlund, 1980), but this unit, here named the KN78 rhyolite, has an 40Ar/39Ar date of 34.0 ± 0.2 Ma (McIntosh et al., 1991), making it correlative with a series of coeval MDVF tuffs collectively known as the Box Canyon Tuff. The youngest unit is the 32.6 ± 0.4 Ma Malpais Hills basaltic trachyandesite lava flow.

Most of the volcanic units contained zircons reflecting inheritance from ca. 1.6 Ga Mazatzal province rocks, ca. 1.45 Ga A-type granites, and ca. 1.2 Ga Grenville igneous rocks, as well as minor Paleogene zircons derived from Laramide igneous rocks. The abundance of xenocrystic zircon implies significant contamination of magmas by crustal rocks. The sequence at Knight Peak represents magmatism from a typical cycle in the Mogollon-Datil and Boot Heel volcanic fields, beginning with a trachyte followed by massive crystal-poor rhyolite followed by a crystal-rich eruption (KN78) and finishing with a basaltic trachyandesite flow. These new data allow for the Knight Peak sequence to be placed in context with magmatism in adjacent volcanic fields. The entire volcanic section, plus the base of the overlying Miocene to Pliocene (?) Gila Conglomerate, is tilted 30–45° to the northeast on the southwest-dipping Knight Peak normal fault. This suggests that the Basin and Range topography in this area formed in the Miocene, consistent with previously published thermochronology, which demonstrates Oligocene–Miocene cooling of exhumed basement and confirms the postulated Miocene age for the lower Gila Conglomerate that fills half grabens in the hanging wall of Basin and Range normal faults.

#### Introduction

The Knight Peak region of southwestern New Mexico exposes a series of volcanic rocks with a total thickness of approximately 1100 m and comprising four mapped volcanic units (Hedlund, 1980). These outflow sheets and lava flows lie within the Mogollon-Datil volcanic field (MDVF; e.g., Chapin et al., 2004), which was part of the widespread Cenozoic ignimbrite flare-up (e.g., Coney, 1978; Johnson, 1991; Best et al., 2016). Magmatism during this event followed late Laramide intermediate volcanism in the region related to subduction of a shallowly dipping, but not flat, oceanic slab (see summary in Amato et al., 2017). Magmatism in the MDVF was generated from 13 calderas over an area spanning approximately 36,000 km<sup>2</sup>, ranging in age from approximately 36 to 24 Ma (Fig. 1; McIntosh et al., 1992; Chapin et al., 2004). The study area was originally described by Ballmann (1960); it crops out within the Redrock SE 1:24,000 quadrangle (Eagle Eye Peak quadrangle in 1990), which was mapped by Hedlund (1980). Despite the extensive 40Ar/39Ar geochronologic investigations of volcanism in the MDVF (McIntosh et al., 1991, 1992) and in the Boot Heel volcanic field (BHVF; McIntosh and Bryan, 2000), only one radiometric age has been published from this section of lava flows and outflow sheets (tuff KN78; McIntosh et al., 1991).

The origin of the ignimbrite flare-up has been related to slab rollback (Coney and Reynolds, 1977) or slab breakoff (Humphreys et al., 2003), followed by heating of the lithosphere (Farmer et al., 2008). The latest Laramide intermediate volcanism occurred at 40 Ma (McMillan, 2004), and voluminous rhyolite ignimbrites in the region began to be erupted around 36 Ma (McIntosh et al., 1991). The majority of felsic ash-flow tuffs erupted during the earliest phase of the MDVF, from 36 to 34 Ma (Vermillion et al., 2024).

One reason the rocks of the Knight Peak region have not been dated is that there are several low-SiO $_2$  units, including a trachyte and an andesite, that in the study area lack minerals dateable with the  $^{40}$ Ar/ $^{39}$ Ar method. Given the low cost and rapid data acquisition advantages of laser ablation inductively coupled plasma mass spectrometry (LA-ICPMS) on zircons, we used this method to obtain U-Pb dates of zircons from tuffs and lava flows. The goal of this project was to determine the ages of the volcanic rocks in this sequence, to attempt to trace these outflow sheets to nearby calderas and/or correlate them to other dated tuffs, and to determine their structural history. All previously published  $^{40}$ Ar/ $^{39}$ Ar dates mentioned in the text have been recalculated using the updated age of the Fish Canyon Tuff standard (28.201 Ma; Kuiper et al., 2008).

## **Background Geology**

The Knight Peak area of southwestern New Mexico lies approximately 25 km northeast of the town of Lordsburg and 35 km southwest of Silver City. The main structural element is a basement high cored by Proterozoic granite and metamorphic rocks and covered unconformably by tilted Eocene-Oligocene volcanic rocks. This region lies within the southern part of the MDVF (McIntosh et al., 1992) and northeast of the BHVF (McIntosh and Bryan, 2000). The nearest calderas are the Schoolhouse Mountain, Twin Sisters, and Emory calderas of the MDVF and the Muir and Steins calderas of the BHVF (Fig. 1). To the northeast and southwest of the study area, Paleozoic sedimentary rocks are lying nonconformably on Proterozoic basement (Drewes et al., 1985), and mid-Cretaceous sedimentary rocks lie on Proterozoic basement to the north of the study area (Lawton et al., 2020) and on Paleozoic rocks to the northeast of the study area (Drewes et al., 1985), but Paleozoic and mid-Cretaceous rocks are absent from the Knight Peak block (Fig. 2A).

This part of southwestern New Mexico is characterized by Basin and Range topography with a NNW-SSE orientation of the structures, which is evident in the topography as well as the gravity and aeromagnetic data (Fig. 2A; Kucks et al., 2001). The regional relationships show that the rocks of the study area crop out in a Basin and Range uplift that we are calling the Eagle Eye Peak block, located southwest of the Burro Peak block (Fig. 2A). A cross section through this region (Fig. 2B) shows the volcanic rocks making up a broad anticline. When restored to the time when the volcanic rocks were flat (Fig. 2C), Paleozoic and Cretaceous sedimentary rocks also form an anticline likely related to Laramide deformation.

The principal normal faults that control the regional structure are, for the most part, covered by Quaternary deposits, and modern seismicity is low: no natural earthquakes have been recorded in the area covered by Figure 2A since 1980. The unexposed Knight Peak normal fault is interpreted to dip around 45° to the southwest. This relatively low dip for a normal fault is required in order to be able to restore the dipping beds in the hanging wall to horizontal and still retain a normal fault geometry (Figs. 2B and 3B). There is another parallel normal fault <1 km to the southwest of the Knight Peak fault, which is exposed north of the area shown in Figure 3A (see inset box in Fig. 2A). The volcanic strata at Knight Peak strike northwest and dip 30-45° to the northeast (Hedlund, 1980, and supplemental data from this study; Fig. 3A), but most of the units dip at angles closer to 40° (Fig. 3A). They are bounded on the southwest by Proterozoic granite of the Burro Mountains intrusive suite (e.g., Gaynor, 2013), which has been dated to ca. 1.46 Ga (Amato et al., 2011). The tilting is inferred to result from a normal fault active during Basin and Range extension (Fig. 3B). Hedlund (1980) mapped the "Knight Peak Fault" striking N30W and dipping to the southwest between the tilted volcanic section of interest and Proterozoic granite exposures in the footwall (Fig. 2A). There are likely other unexposed faults beneath the younger deposits.

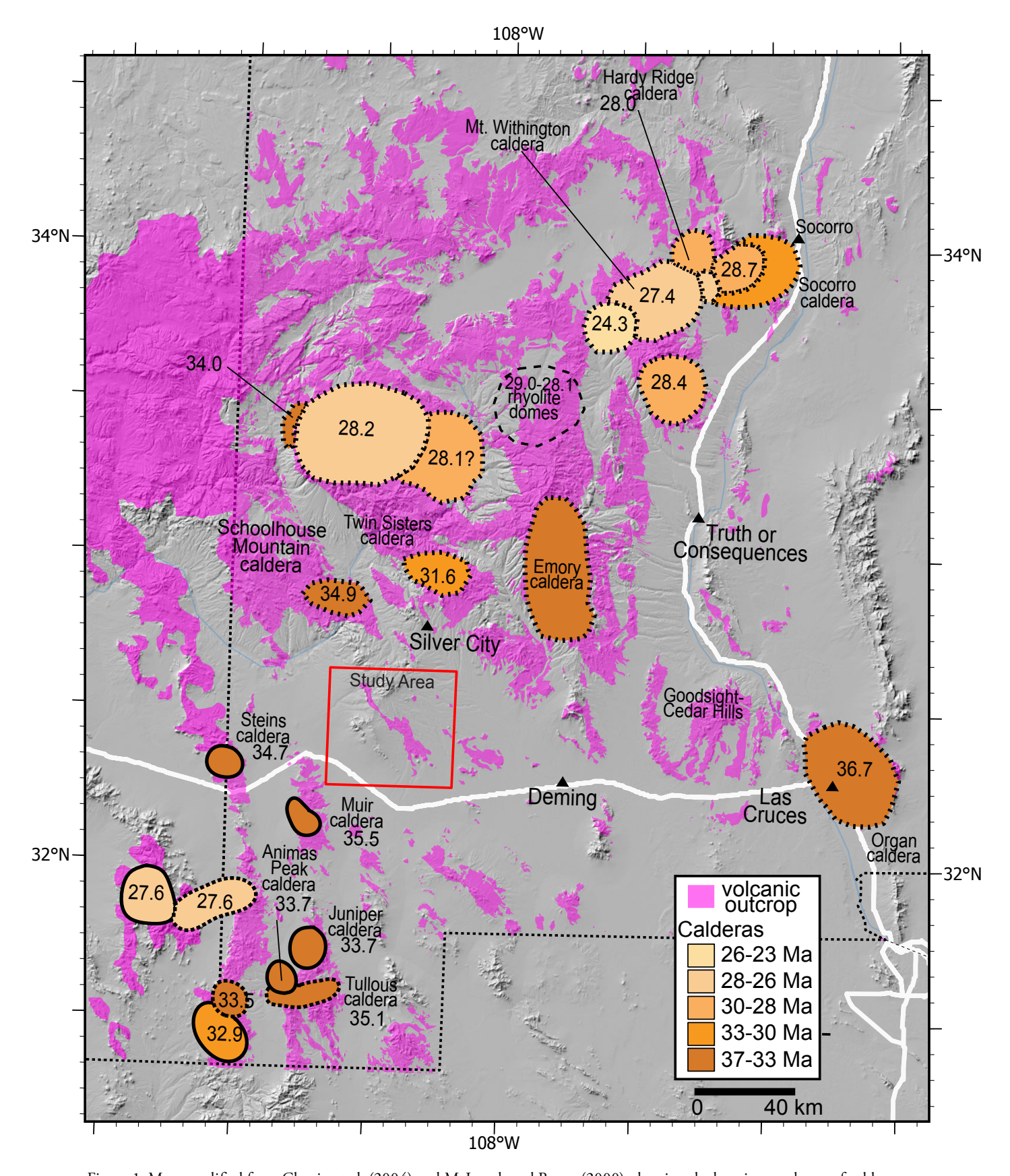


Figure 1. Map, modified from Chapin et al. (2004) and McIntosh and Bryan (2000), showing the locations and ages of calderas within the Mogollon-Datil and Boot Heel volcanic fields. Visible caldera boundaries are shown by solid lines and inferred boundaries by dashed lines. Triangles show cities. Red box shows the area of Knight Peak (see Fig. 2A). Age of the Schoolhouse Mountain caldera is updated from Swenton (2017). Geologic base maps are from New Mexico Bureau of Geology and Mineral Resources (2003) and Richard et al. (2002).

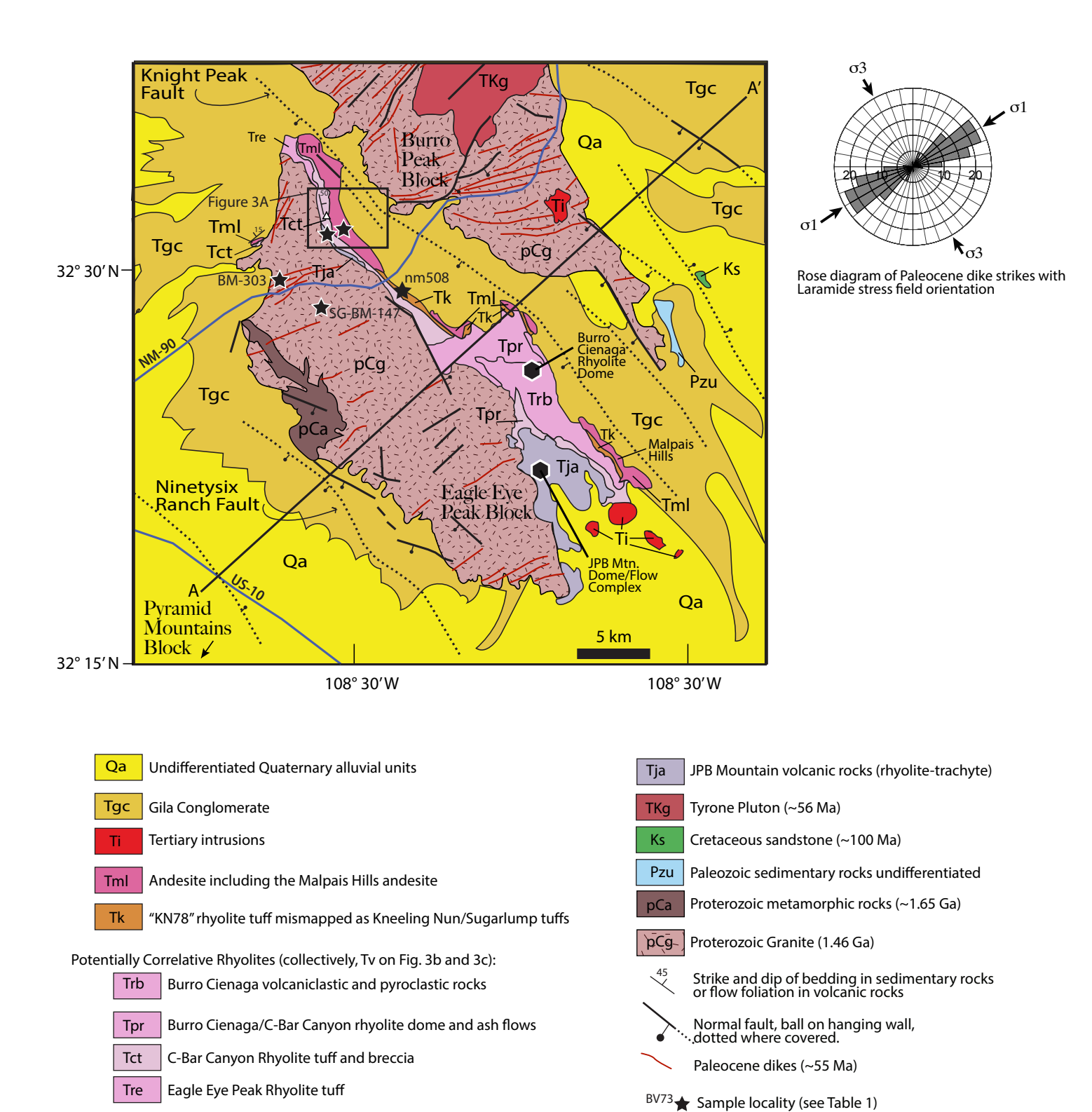


Figure 2A. General geologic map of the region showing two main fault blocks cored by Proterozoic granite and metamorphic rocks. The location of Figure 3A is shown in the black box. Also shown is the approximate location of geochronology sample nm508 from McIntosh et al. (1991). Geology was modified and simplified from Drewes et al. (1985); cross section along line A–A' is shown in Figure 2B.

△ Knight Peak

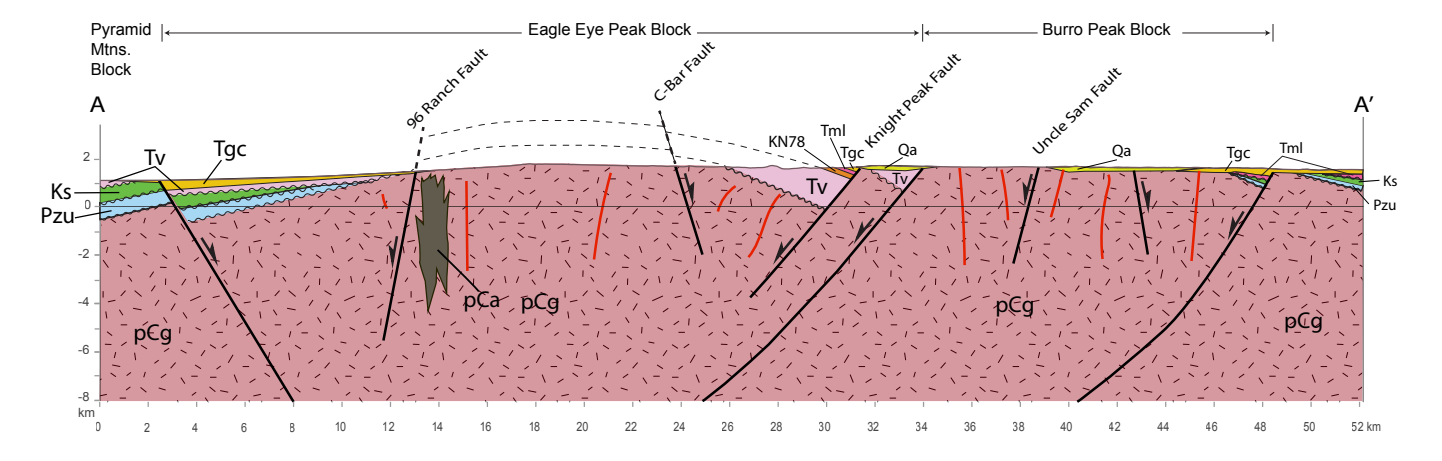


Figure 2B. Cross section across line shown in Figure 2A based on map of Drewes et al. (1985), supplemented with interpretations based on geophysical data (Kucks et al., 2001) and detailed mapping from Hedlund (1980). Red lines are dikes, thick black lines are faults.

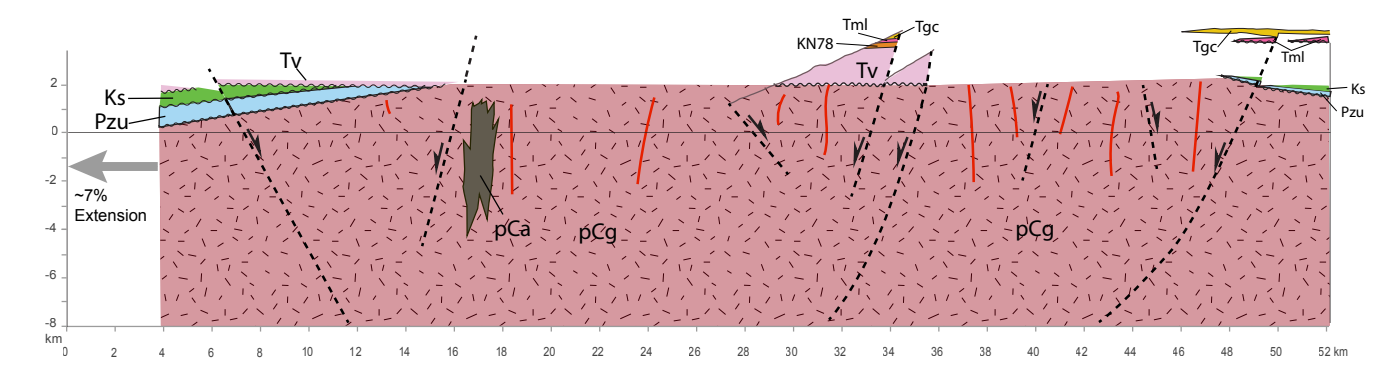


Figure 2C. Restoration of section shown in Figure 2B at 36–32 Ma, with flat-lying volcanic rocks deposited unconformably over the Cretaceous and Paleozoic sedimentary rocks and basement. Note that the Paleozoic and Cretaceous sandstone units do not crop out in the study area (Fig. 3A; box), that those units are broadly folded into an anticline across the region (likely during the Laramide orogeny), and that the total extension on Basin and Range normal faults is calculated at around 7%.

The Phanerozoic units were deposited nonconformably over the Proterozoic granite (Fig. 3B). The oldest of these units (TKk; all map symbols and thicknesses are from Hedlund, 1980) is an arkosic sandstone and pebble conglomerate composed mainly of clasts derived from the underlying granite. It is exposed over a map distance of 1 km and pinches out to the northwest and southeast, with a thickness of about 50 m where it crosses Knight Canyon. This was tentatively correlated to the Lobo Formation by Ballmann (1960) and mapped as Late Cretaceous/ Paleocene by Hedlund (1980). However, based on its limited lateral distribution, we consider it to be more likely Paleogene and related to deposition in the basin just prior to volcanism. A series of rhyolite dikes that do not cut the volcanic sequence (unit Tr; up to 15 m thick; Fig. 2A) was mapped in the area in and around Knight Peak by Hedlund (e.g., 1978d, 1980). These were inferred to have an Eocene and/or Paleocene age (Hedlund, 1978c). The strikes of these dikes average N60E (Fig. 2A). We sampled one of these previously undated dikes for geochronology.

The oldest volcanic units in the sequence are the felsic tuff and andesitic lava flow of JPB Mountain. The tuff (Tjat) is approximately 25–30 m thick and contains pumice fragments. Overlying this is a series of lava flows up to 100 m thick mapped

as andesite (Tja). Our new geochemical analyses show that this unit is not andesite. Instead, we refer to it as the JPB Mountain trachyte. These units are part of a group of flows and tuffs associated with the JPB Mountain dome and flow complex and named for JPB Mountain in the southern part of the Werney Hill quadrangle (Hedlund, 1978a). This unit is 80–100 m thick along the cross-section line in our study area (Fig. 3B).

The next units up section are the "Tuff (Tct) and pyroclastic breccia (Tctb) of C-Bar Canyon," here referred to as the tuff and tuff breccia of C-Bar Canyon (Fig. 3A). These two units combine for a regional maximum thickness of 680 m (Hedlund, 1980). In the study area, these units combine to a thickness of 400–450 m, with the breccia unit making up the summit of Knight Peak, but the tuff units both pinch out to the north where the "Rhyolite of Eagle Eye Peak" (Tre; 130 m), referred to here as the Eagle Eye Peak rhyolite, occupies the same stratigraphic interval. The C-Bar Canyon tuff ends to the south in the central C-Bar Ranch quadrangle (Hedlund, 1978b), where the Burro Cienaga rhyolite units are locally mapped and inferred to be correlative in age based on their similar stratigraphic position. The Burro Cienaga rhyolites are mapped as a dome and flow complex in the Werney Hill quadrangle (Hedlund, 1978a).

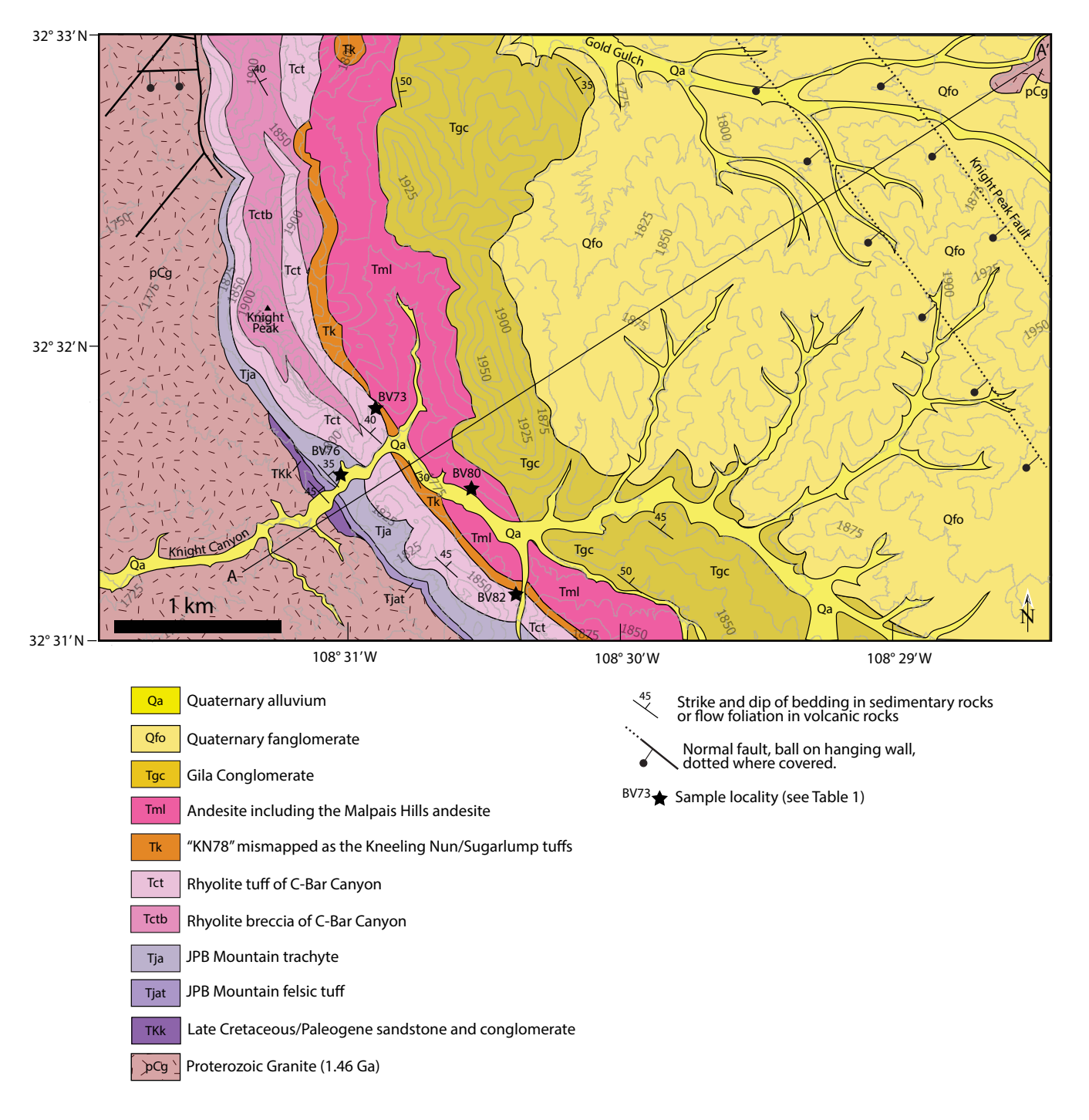


Figure 3A. Simplified geologic map of the Knight Peak region (modified from Hedlund, 1980). Key modifications include adding another normal fault southwest of the Knight Peak fault (extrapolated from north of the map area) and inferring a contact between units Tgc and Qfo that was not originally mapped across the map boundary. Contour interval is 25 m.

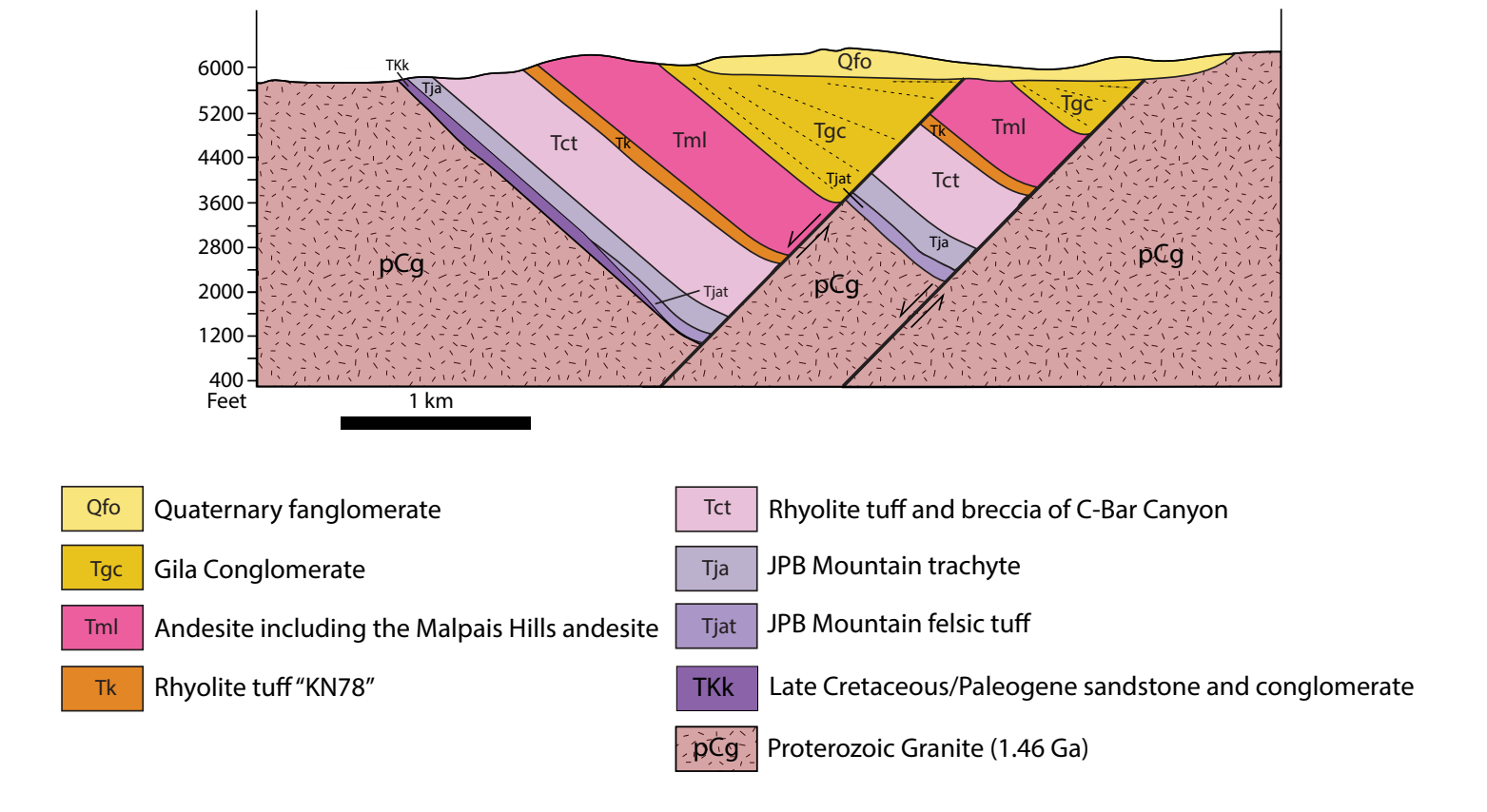


Figure 3B. Cross section across line A–A' shown in Figure 3A. Dips of the volcanic sequence are shown at around 40°, which is representative regionally. Decreasing dips in unit Tgc moving to the west indicate growth strata. In this interpretation, all of the tilting of the volcanic section is the result of movement on these Basin and Range normal faults.

Overlying this is a unit mapped as Kneeling Nun Tuff (Tk; 25 m; Fig. 3A); we are referring to this unit as the "KN78 tuff" (based on the original mapping name of Kneeling Nun and a dated sample in an adjacent quadrangle published by Hedlund, 1978c) because its age of  $34.03 \pm 0.24$  Ma ( $^{40}$ Ar/ $^{39}$ Ar by McIntosh et al., 1991; sample nm508; Fig. 2A) is not correlative with the Kneeling Nun Tuff (e.g., Elston et al., 1975), which is older at  $35.36 \pm 0.04$  Ma (McIntosh et al., 1991). KN78 tuff is 50 m thick in the study area.

The youngest unit in this volcanic sequence is the "Latite and Andesite of Malpais Hills" (Tml; 180 m), referred to here as the Malpais Hills basaltic trachyandesite. This unit is at least 225 m thick in our study area (Fig. 3B) and appears to be a series of thick lava flows.

Unconformably overlying the volcanic rocks is a conglomerate/fanglomerate unit variously called the Gila Formation, Gila Conglomerate, or Gila Group (Tgc). This unit is likely middle Miocene to Pliocene in age, but it is possibly early Miocene (Cather et al., 1994; Mack, 2004; Mack and Stout, 2005; Gootee et al., 2021). This sedimentary unit was deposited in grabens west of the Continental Divide. Hedlund (1980) estimated the thickness in the area to be 400–600 m, but Mack (2004)

suggested a thickness of 1000 m based on gravity surveys and well data. We support the 1000 m thickness, which allows us to draw a reasonable cross section through the region (Fig. 3B). The 50° dip of the conglomerate at its base is comparable to that of the underlying volcanic rocks, but up section the beds decrease in dip to 35° and then 30° over a map distance of about 1.5 km, as is expected of syntectonic deposits.

Α'

In the study area, the basal part of these rocks is tilted to approximately the same dip and dip direction as the volcanic strata (Fig. 3B), indicating that the tilting postdates deposition of the basal Gila Conglomerate (Hedlund, 1980). Overlying these rocks is a unit (Qfo) consisting of Pleistocene fan deposits more than 60 m thick (Hedlund, 1980). These deposits are apparently not tilted, and they are incised by modern drainages (Qa; Fig. 3A). These were inconsistently mapped by Hedlund (1978c, 1980), and the contact between them is not obvious; we relocated this contact (Fig. 3A) based on field relationships and the cross-section geometry.

Overall, this stratigraphic succession consists of approximately 1100 m of Paleogene volcanic rocks overlain by nearly 1000 m of Miocene–Pliocene Gila Conglomerate and Quaternary deposits (Fig. 4).

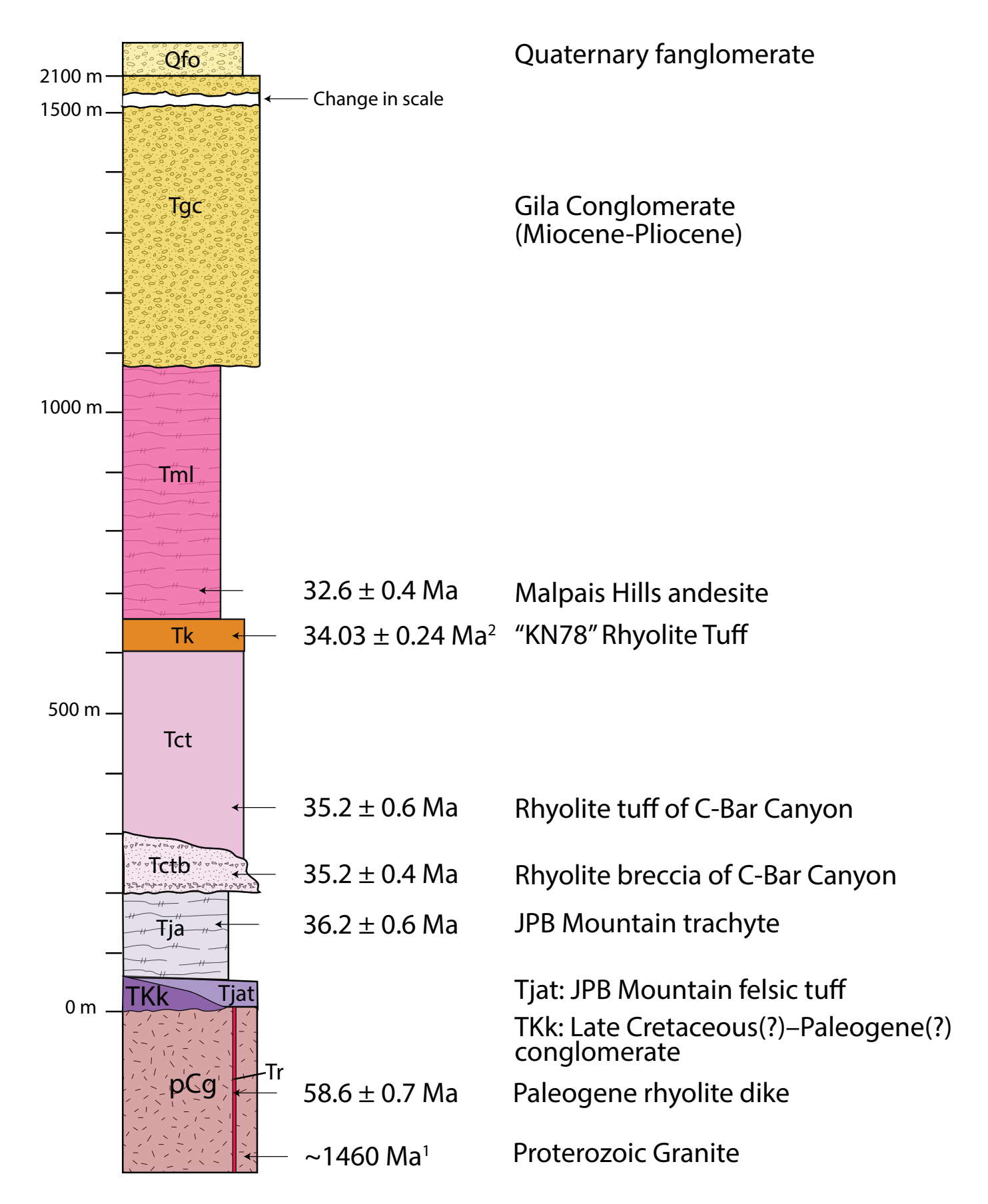


Figure 4. Schematic stratigraphic column for units discussed in text. Approximate thicknesses measured from geologic map (Hedlund, 1980). Total thickness of unit Tgc is likely closer to 1000 m (see Fig. 3B and text). Ages are weighted mean <sup>238</sup>U/<sup>206</sup>Pb zircon ages from this study, discussed in the *Geochronology* section below, except for units pCg (1: Amato et al., 2011) and Tk (2: McIntosh et al., 1991).

#### Methods

#### Fieldwork

Fieldwork was conducted in 2015–2016 and in 2025. We collected 23 samples, mainly along a transect south of Knight Peak in and around Knight Canyon. Most structural relationships were interpreted based on previous mapping (e.g., Hedlund 1978a, 1978b, 1978c, 1978d, 1980), with some new measurements.

### U-Pb Geochronology

We conducted U-Pb dating of zircons using laser ablation inductively coupled plasma mass spectrometry (LA-ICPMS) at the Arizona LaserChron Center at the University of Arizona. We chose this method over 40Ar/39Ar because the trachyte and andesite units lacked sufficient sanidine. Similarly, the tuff of C-Bar Canyon is crystal-poor, and we did not recover sanidine from the three samples for which we attempted separations. Zircons were concentrated using standard techniques (crushing, disc mill, Gemini table, Frantz, and heavy liquid steps at 2.85 g/cm<sup>3</sup> and 3.3 g/cm<sup>3</sup>, followed by sieving to <250 mm). We used a single-collector Element 2 mass spectrometer with a 20 mm beam diameter following the methods described in Pullen et al. (2018). Rims of zircons were preferentially analyzed, but for small zircons we analyzed the core. We filtered out analyses with >10% uncertainty and >10% discordance. We report all ages in the text at the  $2\sigma$  level. The mean square of weighted deviates (MSWD) is reported for each sample. All weighted mean uncertainties include both random and systematic errors. Weighted mean plots were made using IsoplotR (Vermeesch, 2018). A summary of the ages and sample locations is shown in Table 1<sup>1</sup>, and the entire analytical dataset is in Table 2.

#### Geochemistry

Whole-rock geochemistry was obtained using a Rigaku ZSX Primus II X-ray fluorescence (XRF) spectrometer at New Mexico State University (NMSU). Some samples were analyzed at the Peter Hooper GeoAnalytical Lab at Washington State University using a Thermo-ARL automated XRF spectrometer. Samples were powdered using a tungsten carbide shatterbox. Glass beads were made with a lithium borate flux. Trace element concentrations were determined using pressed pellets created from powdered sample and a binding agent. The standard AGV-2 provided by NMSU was analyzed for both glass beads and pressed pellets. All major element graphs were made with the data normalized to 100% anhydrous. Accuracy on major element concentrations was within 1.1% of established values. Volcanic classifications were made using a total alkali-silica diagram (Le Bas et al., 1992) or phenocryst compositions. Geochemical data are reported in Table 3.

### Unit Descriptions and Geochemistry

#### JPB Mountain Sequence

We dated a lava flow from the JPB Mountain sequence. In outcrop and hand sample (Fig. 5B), the unit is medium to dark gray and contains linear, red-brown, weathered patterns. The sample is porphyritic (Figs. 6A and 6B), with about 15% total phenocrysts in a groundmass of plagioclase microlites weakly oriented along flow textures. The phenocrysts are highly altered and dominantly consist of <0.5 mm subhedral amphibole with minor subhedral to anhedral plagioclase, clinopyroxene, and orthopyroxene. The amphibole phenocrysts are aligned with the foliation. The analyzed sample has SiO<sub>2</sub> of 61.7 wt%, Fe<sub>2</sub>O<sub>3</sub> of 5.7 wt%, Na<sub>2</sub>O of 5.2 wt%, and K<sub>2</sub>O of 3.0 wt%. This classifies as a trachyte.

Underlying this unit is a highly altered thin ignimbrite of intermediate composition (Tjat), which is the lowermost volcanic rock sequence exposed west of Knight Peak. It is thickest to the south and pinches out just south of Knight Canyon. The ignimbrite crops out over a map distance of about 2 km (Hedlund, 1980). We did not date this tuff.

#### C-Bar Canyon Rhyolite Sequence

The cliff-forming C-Bar Canyon rhyolite tuff sequence comprises two units. The tuff breccia (Tctb) is a light-yellow to cream, poorly to moderately welded, lithic-rich pyroclastic flow that forms the ridgeline of the Knight Peak block (Fig. 2A). Matrix material is altered and stained brown and green in areas of great weathering, particularly where there is abundant biotite and pumice (Figs. 5C, 5D, 6C, and 6D). Lithic fragments range from 3 mm to 20 cm and consist of crystal-rich rhyolite, flow-banded rhyolite, and trachyte similar to the underlying JPB Mountain unit. Lithic clast abundance remains consistent, but clast sizes decrease from the bottom to the top of the unit. Pumice clasts are about 1 cm wide and are slightly compacted at the bottom of the unit. Going north-northwest along strike from Knight Peak, clast sizes and abundance decrease, with the majority of the clasts being ≤1 cm. This sample has a matrix of devitrified and altered ash (Fig. 6C) and has phenocrysts that are <5% by volume, dominated by plagioclase with minor quartz and altered biotite, with trace altered sanidine.

Interbedded with the tuff breccia are layers of greenish-white to pinkish-cream rhyolite ash-flow tuff (Tct; Fig. 5E) with a highly weathered, moderately to poorly welded matrix (Fig. 6D). The ashy matrix contains around 10% phenocrysts with compositions including highly altered subhedral to anhedral quartz, biotite, and sanidine (≤0.2 mm). Lithic fragments (-10%) are 1–5 mm clasts of crystal-rich rhyolite, quartzite, and flow-banded rhyolite. Minor Fe-Ti oxides (<2%) and microcrystalline veins are present in thin section. Multiple samples were processed to obtain sanidine for <sup>40</sup>Ar/<sup>39</sup>Ar dating, but none was recovered.

<sup>&</sup>lt;sup>1</sup> Tables are available for download at https://geoinfo.nmt.edu/repository/index.cfml?rid=20250003

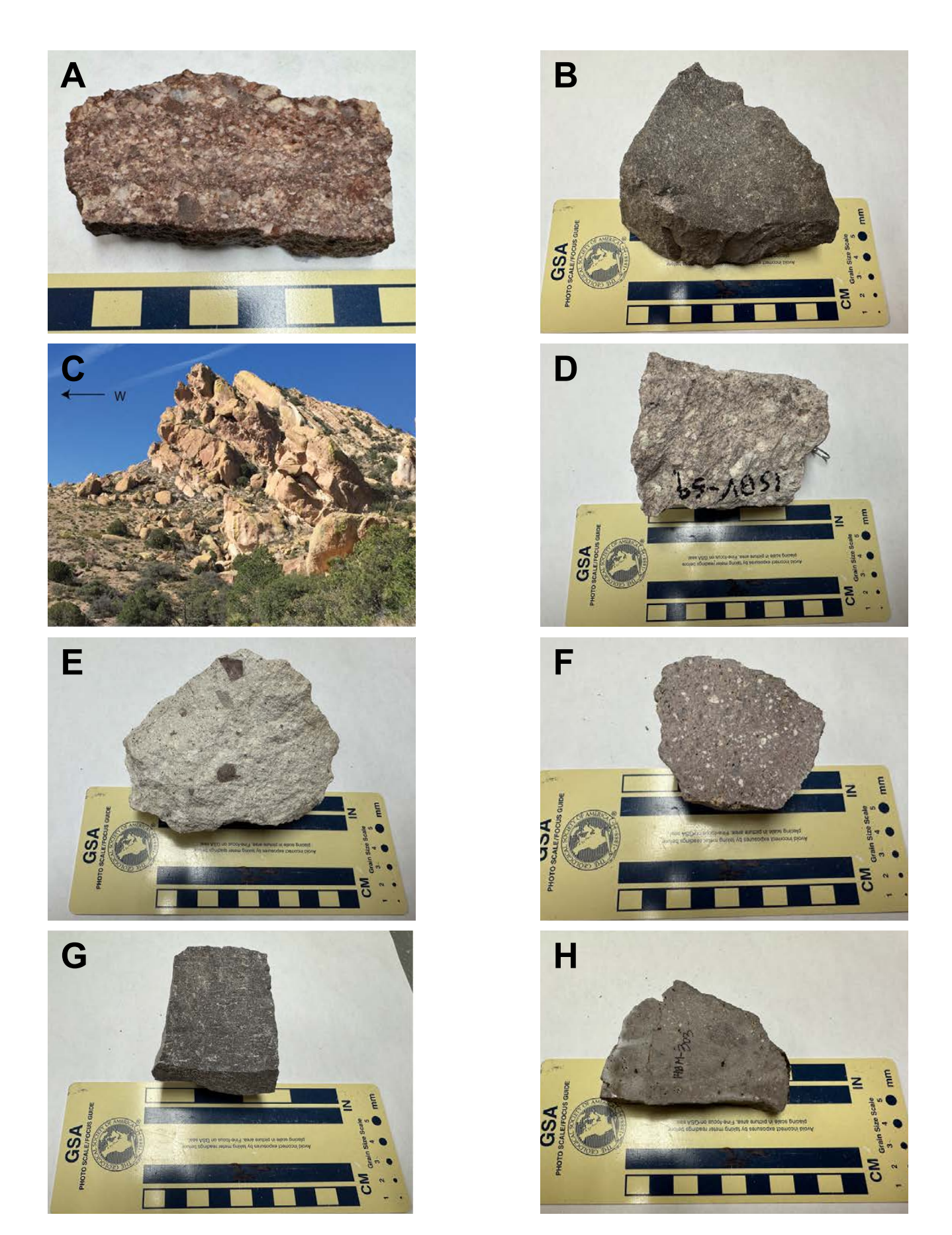


Figure 5. Photographs of (A) sample of conglomerate (unit TKk) from above Proterozoic granite and below volcanic rocks; (B) sample of JPB Mountain trachyte; (C) side view of C-Bar Canyon rhyolite breccia and tuff, view to the north; (D) sample of C-Bar Canyon breccia; (E) sample of C-Bar Canyon tuff with dark lithic fragments; (F) sample of KN78 rhyolite tuff; (G) sample of Malpais Hills basaltic trachyandesite; and (H) sample of Paleogene rhyolite dike.

# KN78 Rhyolite Tuff ("Kneeling Nun Tuff" of Hedlund, 1978c)

The KN78 rhyolite unit is a grayish purple-red, moderately welded, crystal-rich ignimbrite (Fig. 5F). This unit is composed of around 30% phenocrysts ranging from 0.5 to 3.5 mm in diameter. Plagioclase phenocrysts (10%) are skeletal, euhedral to subhedral, and up to 3.5 mm in length. Quartz (15%) phenocrysts are up to 3 mm in length and bipyramidal, and some crystal edges are resorbed. Biotite flakes (1%) are euhedral and up to 1 mm across. Sanidine (5%) is about 1 mm across. The matrix is poorly welded and microcrystalline and contains abundant glassy bubble-wall ash fragments (Figs. 6E and 6F). This sample has SiO<sub>2</sub> of 76.9 wt% and low Fe<sub>2</sub>O<sub>3</sub>, MgO, Mn, and Ti. It has Na<sub>2</sub>O of 2.7 wt% and K<sub>2</sub>O of 5.1 wt%, classifying it as a rhyolite.

#### Malpais Hills Basaltic Trachyandesite

Exposed on the eastern side of Knight Peak is a medium-gray, aphanitic andesite flow unit mapped as the Malpais Hills andesite (Fig. 3A). Flow textures are observed in outcrop and hand sample (Fig. 5G), which can be seen as small, flow-oriented plagioclase laths and glomerocrysts in thin section (Figs. 6G and 6H). Phenocrysts (~15%) include clinopyroxene and orthopyroxene (~5%), plagioclase (~5%), Fe-Ti oxides (5%), and minor zircon. Pyroxene and plagioclase crystals are subhedral to anhedral, fragmented, and  $\leq$ 1.5 mm. Fe-Ti oxides are anhedral and  $\leq$ 0.5 mm. A sample from this unit has SiO<sub>2</sub> of 56.2 wt%, Fe<sub>2</sub>O<sub>3</sub> of 7.8 wt%, high CaO and MgO, and low Na<sub>2</sub>O and K<sub>2</sub>O, placing it in the basaltic trachyandesite field of a total alkali-silica diagram.

#### Rhyolite Dikes (Tr)

The rhyolite was sampled from a 3-m-wide dike striking approximately S50W and dipping to the northwest, located approximately 5 km southeast of Knight Peak (Fig. 2A). The sample is leucocratic with minor (<3%) phenocrysts, including equant subhedral to rounded quartz phenocrysts and minor plagioclase phenocrysts within a microcrystalline groundmass. The groundmass also contains muscovite.

## **U-Pb Geochronology Results**

We dated zircons from five samples using LA-ICPMS. Most samples had a mix of magmatic and inherited zircons. Note that the uncertainties on the ages (approximately 1–2%) preclude any interpretation as to whether the zircon ages may be slightly older than the eruption ages. The age results are presented from oldest to youngest (Fig. 7).

A sample (14BM-303) from the rhyolite dike intruding the Proterozoic granite yielded 38 igneous grains that resulted in a weighted mean  $^{238}\text{U}/^{206}\text{Pb}$  age of 58.6 ± 0.6 Ma (Fig. 7A; n=38; MSWD=0.6). One Proterozoic zircon had an age of 1487 ± 34 Ma. A sample (15BV-76) from the JPB Mountain trachyte flow yielded an age of  $36.2 \pm 0.6$  Ma (Fig. 7B; n=8, MSWD=0.3). This sample also had three populations of inherited Proterozoic zircons: 16 late Mesoproterozoic zircons yielded a weighted mean <sup>207</sup>Pb/<sup>206</sup>Pb age of 1217 ± 15 Ma, and older grains were 1420 Ma, 1482 Ma, and 1610 Ma. We analyzed 54 zircons from the C-Bar Canyon rhyolite breccia (sample 16BV-82; Fig. 7C), and 30 of these formed a young population inferred to be the eruption age at  $35.2 \pm 0.4$  Ma (n=30; MSWD=1.7). One grain had an age of 56 Ma. The 20 grains dated ca. 1.4 Ga yield a weighted mean <sup>207</sup>Pb/<sup>206</sup>Pb age of 1453 ± 17 Ma. One zircon had an age of 1602 Ma. A sample from the C-Bar Canyon rhyolite tuff unit (sample 15BV-73; Fig. 7D) overlying the tuff breccia yielded an age of 35.2  $\pm$  0.6 Ma (n=12; MSWD=0.3). This sample also had 21 Proterozoic zircons ranging in age from 1400 to 1700 Ma. The highest stratigraphic unit, the Malpais Hills andesite, yielded no inherited grains (Fig. 7E). Of the 35 apparently magmatic grains, one was rejected for being slightly older than the main group, which had a weighted mean  $^{238}$ U/ $^{206}$ Pb age of 32.6 ± 0.4 Ma (n=34; MSWD=0.2).

Summarizing these ages, the rhyolite dike is significantly older than the volcanic strata near Knight Peak. The U-Pb zircon weighted mean ages become younger up section, from the ca. 36 Ma JPB Mountain trachyte to the youngest Malpais Hills basaltic trachyandesite at ca. 33 Ma. Both samples of the C-Bar Canyon rhyolite were 35.2 Ma. Most samples had inherited Proterozoic zircons, with the JPB Mountain trachyte being the only sample with ca. 1.2 Ga ages. All samples with Proterozoic zircons had ca. 1.45 Ga ages represented. The generally low (<1.0) MSWD values indicate that the individual uncertainties are overestimated, but this does not affect the age interpretation.

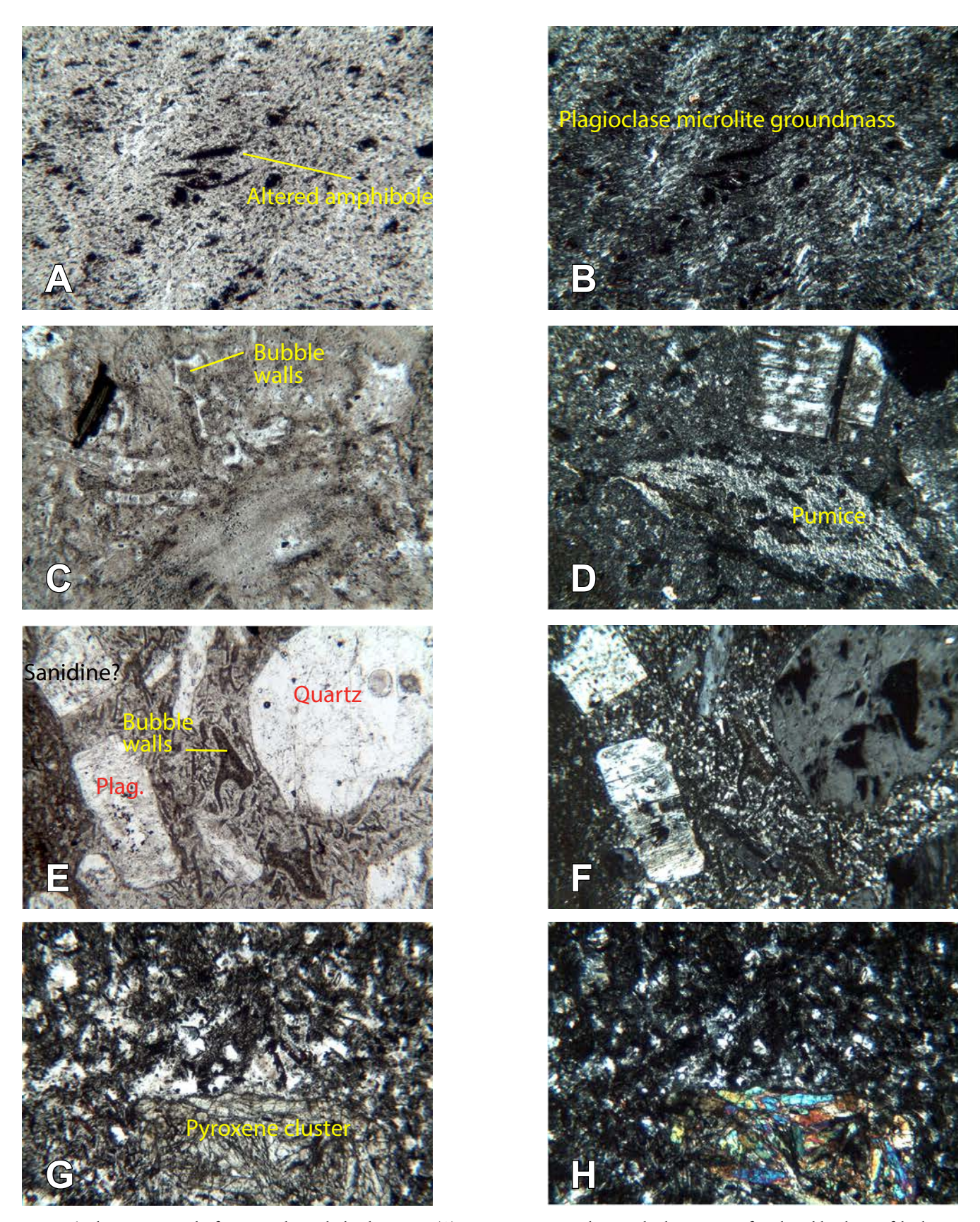
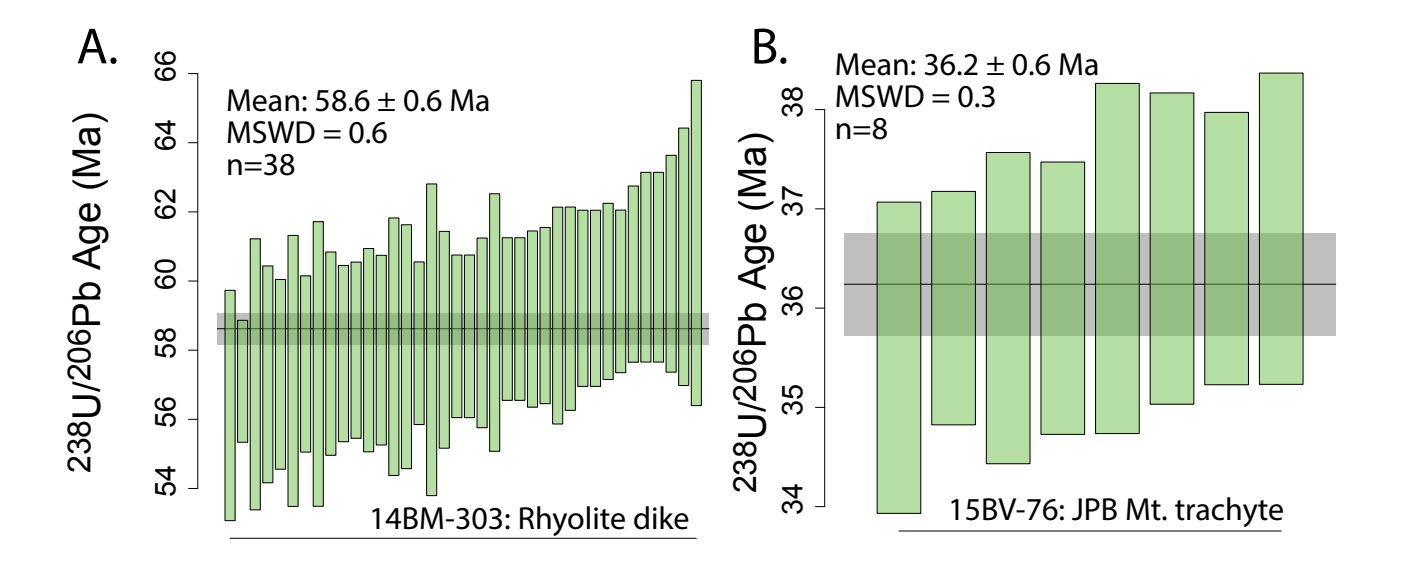
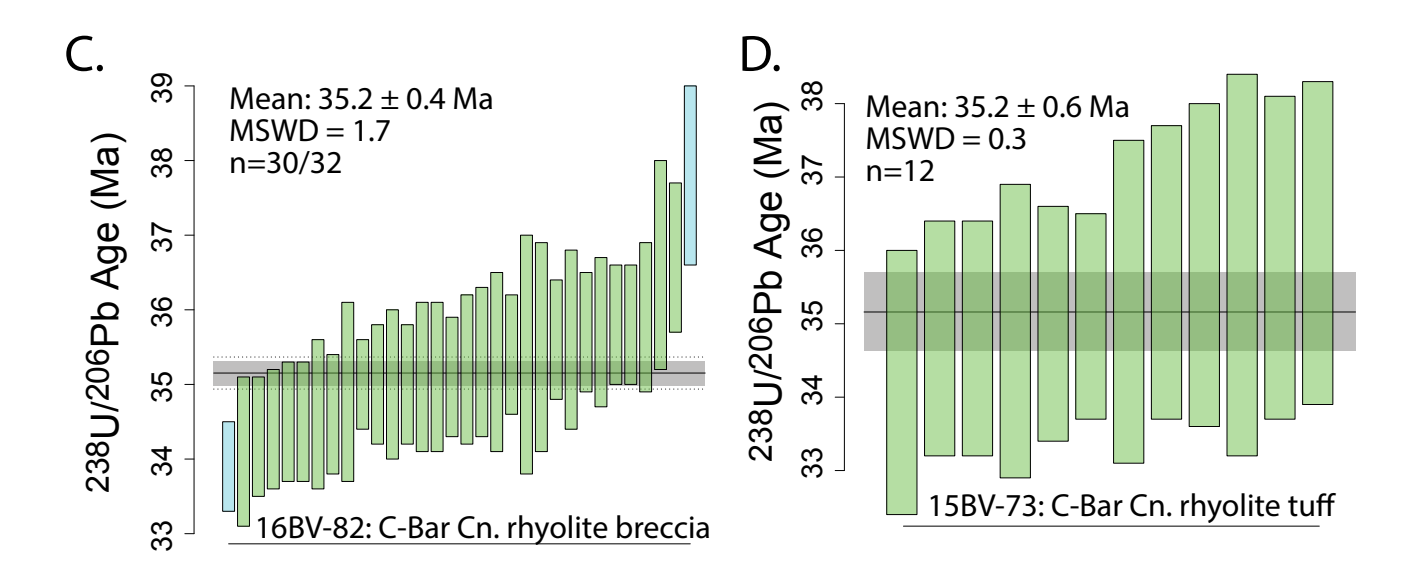
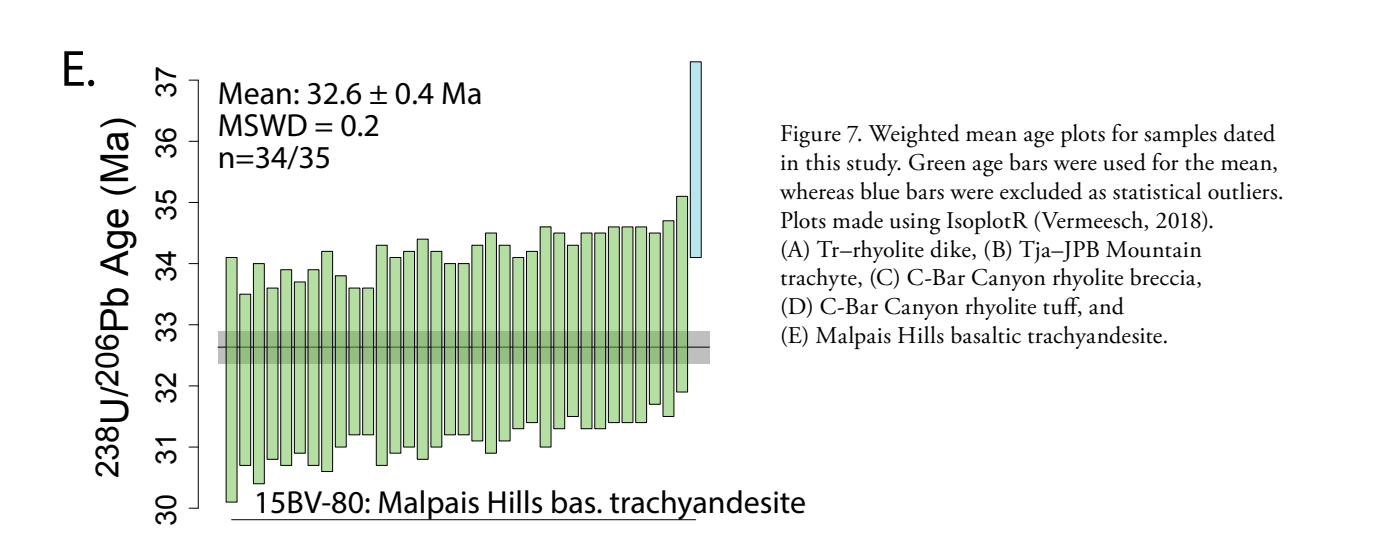


Figure 6. Photomicrographs from Knight Peak rhyolite units. (A) JPB Mountain trachyte with phenocrysts of oxyhornblende in a felted matrix of plagioclase laths; (B) same photo as Figure 6A under crossed polars; (C) C-Bar Canyon rhyolite, with glassy bubble-wall fragments; (D) C-Bar Canyon rhyolite, showing plagioclase phenocryst and pumice fragment, under crossed polars; (E) KN78 rhyolite tuff, showing quartz, plagioclase, and sanidine phenocrysts along with bubble-wall fragments; (F) same photo as Figure 6E under crossed polars; (G) Malpais Hills basaltic trachyandesite with possible xenocryst at bottom center; and (H) same photo as Figure 6G under crossed polars. All photos are 2.5 mm across.







#### Discussion

#### Magmatic History

None of the units within this sequence have been previously correlated to source calderas, nor have they been correlated to other outflow sheets outside of the immediate vicinity of their exposures because they can be traced into adjacent quadrangles. We use our new ages to compare them to existing geochronology of volcanic rocks of similar age in the Mogollon-Datil and Boot Heel volcanic fields (Fig. 8). Note that correlations to the Bell Top Formation tuffs of Clemons (1975) are all abbreviated "BTF" with the tuff number following (e.g., Bell Top Formation Tuff 5 is BTF-5).

The rhyolite dike at ca. 59 Ma is typical of igneous rocks in the Central Mining District of southwestern New Mexico, northwest of Silver City (Mizer et al., 2015). A possible plutonic equivalent in the region south of Knight Peak is the Tyrone pluton at

ca. 58–54 Ma, which is also similar to intrusions associated with ore deposits in eastern Arizona (Stegen et al., 2024). The dikes are more abundant near the stock, but they are not clearly radiating from it.

The trachyte lava flow of JPB Mountain is typical of intermediate eruptions in the MDVF that preceded large rhyolite tuffs (e.g., McIntosh et al., 1991). Its age of  $36.2 \pm 0.6$  Ma overlaps within error of the oldest known volcanic units from the BHVF (Woodhaul Canyon at  $35.7 \pm 0.13$  Ma and Bluff Creek at  $35.6 \pm 0.08$  Ma; McIntosh and Bryan, 2000). This age puts it in the category of some of the other early MDVF eruptions, such as the lower Bell Top Formation tuffs in the Goodsight-Cedar Hills (Fig. 1): BTF-2 at  $36.4 \pm 0.1$  Ma and BTF-3 at  $35.9 \pm 0.01$  Ma. It is also similar to the ages of the Achenbach Park tuff at  $36.26 \pm 0.02$  Ma (Rioux et al., 2016) and the Bar Mountain tuff (formerly SMT Tuff; see Vermillion et al., 2024) at  $36.2 \pm 0.02$  Ma (Rioux et al., 2016), both from the Organ Mountains (Fig. 1). All of these samples are ignimbrites exposed

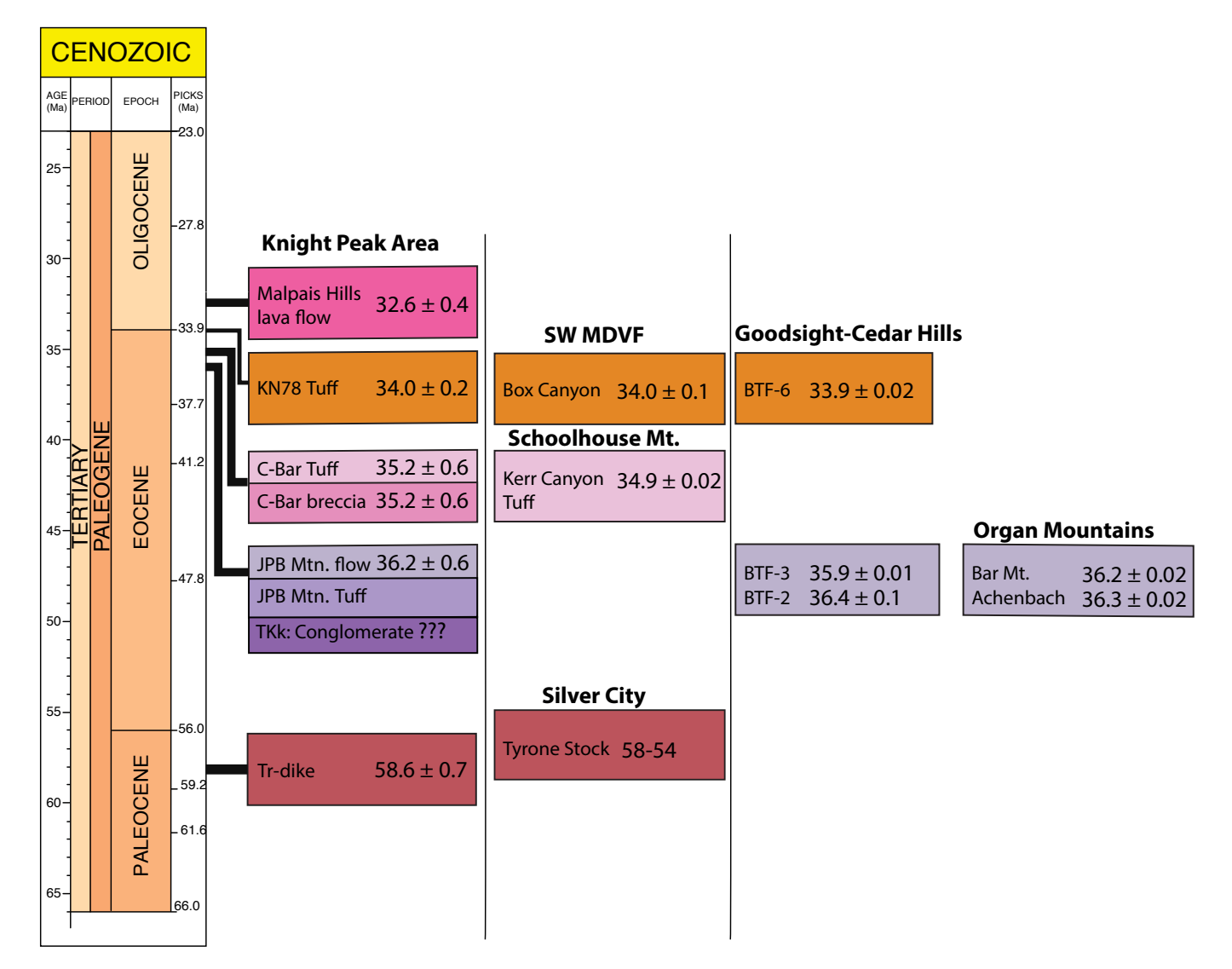


Figure 8. Postulated correlations of volcanic rocks from this study (Knight Peak area). Other areas include the southwestern Mogollon-Datil volcanic field (SW MDVF), the Schoolhouse Mountain caldera (Fig. 1; Swenton, 2017), the Goodsight-Cedar Hills (Clemons, 1975; Vermillion et al., 2024), and the Organ Mountains (Rioux et al., 2016).

100-200 km east of the study area. This trachyte is younger than the volcanic rocks of the underlying Rubio Peak/Palm Park/ Orejon andesite sequence, the youngest sample from which has been dated at  $39.6 \pm 0.5$  Ma (Creitz et al., 2018). Thus, the JPB Mountain flow represents a previously unknown intermediate volcanic unit erupted during the earliest stages of either the MDVF or the BHVF, more than 100 km from the only other known eruptive products of this approximate age from either of these fields. The JPB Mountain trachyte has a composition typical of differentiated parent magmas in continental rifts (e.g., Bhandari et al., 2019; Zheng et al., 2022). Thus, it may represent magma generated during the earliest stages of slab breakoff and asthenospheric upwelling in the MDVF.

The C-Bar Canyon rhyolite tuff and tuff breccia yielded identical ages of 35.2  $\pm$  0.4 and 35.2  $\pm$  0.6 Ma. These dated samples are from a thick section of rhyolite ignimbrites, but the total number of eruptions within this unit is unknown. There were numerous tuffs erupted in the MDVF during this time period, such as BTF-4, BTF-5, and the Kneeling Nun Tuff. However, these do not lithologically resemble the C-Bar Canyon tuffs. The Kerr Canyon tuff, related to the collapse of the Schoolhouse Mountain caldera of the MDVF (Fig. 1), has an age of  $34.9 \pm 0.02$  Ma (Swenton, 2017); it is located less than 30 km from Knight Peak to the north, but it is more crystal-rich than the C-Bar Canyon tuff. Thus, there are no clear candidates for sources of, or correlations to, the most impressive rhyolite ignimbrite in the study area. Crystal-poor ignimbrites such as the C-Bar Canyon unit have been shown to form from extraction from a crystal-rich mush (Bachmann and Bergantz, 2004).

The KN78 tuff at 34.03 ± 0.2 Ma (McIntosh et al., 1991) was correlated with the series of tuffs collectively referred to as the Box Canyon tuff, including Bell Top tuff 6 (BTF-6) in the Goodsight-Cedar Hills and the Cherokee Canyon tuff within the Schoolhouse Mountain caldera (Swenton, 2017), all with ages of approximately 34 Ma (recalculated). These units are all crystal-rich ignimbrites and thus are possible correlations to KN78. Like BTF-6 (Vermillion et al., 2024), KN78 also has low to moderate welding based on the preservation of ash shards. An alternative source from the BHVF could be the Oak Creek tuff at 33.98 ± 0.07 Ma (recalculated from McIntosh and Bryan, 2000), which was derived from the Juniper caldera (Fig. 1).

The Malpais Hills basaltic andesite at 32.6 ± 0.4 Ma falls into an age gap in both the MDVF and BHVF eruptive sequences. Because this unit is made up of lava flows, regional correlations are unlikely, and the lava flow was likely locally derived (e.g., Castruccio and Contreras, 2016). Other undated andesites are reported from the BHVF (e.g., Erb, 1979); for example, an andesite in the southern Animas Mountains is reported to unconformably overlie the Gillespie Tuff, dated at 33.2 Ma (McIntosh and Bryan, 2000), and thus could represent a similar sequence of a thick rhyolite ash-flow tuff followed by an andesite eruption. This unit is likely part of the Southern Cordilleran Basaltic Andesite Suite (SCORBA; Cameron et al., 1989), interpreted as being generated during crustal extension. This

tectonic regime allowed rocks with lower silica concentrations to rise to the surface without modification or contamination (Cameron et al., 1989). This is consistent with the coeval extension and exhumation documented in the southeastern Basin and Range (Gavel et al., 2021).

The unit mapped by Hedlund (1980) as the Eagle Eye Peak rhyolite, rhyolite breccia, and vitrophyre was not dated. This unit pinches out to the south near Knight Peak, raising the possibility that this rhyolite is a different flow unit associated with the C-Bar Canyon rhyolite. If not, the field relationships would imply that the Eagle Eye Peak rhyolite is derived from a northern source within the MDVF. Further work is required to test this hypothesis.

Workers in the region have attempted to identify geographical age trends for the calderas of the MDVF and BHVF. Chapin et al. (2004) grouped the ages of calderas into five age clusters of 2-3 Myr, which loosely implied a pattern of younger ages when moving to the west. However, calderas in the 36-33 Ma group are exposed in the far southeast margin (Organ caldera) of the MDVF, as well as two in the MDVF's farthest west part: the Schoolhouse Mountain caldera at 33.5 Ma, which has been subsequently updated to 34.9 Ma (Swenton, 2017), and the 34.0 Ma Mogollon caldera. Ricketts et al. (2016) used slightly modified age groups to suggest that volcanism broadly progressed from east to west and southeast to northwest. The data may not be of sufficient density to contour the timing of caldera eruptions in the MDVF as indicated by Ricketts et al. (2016). Regardless, the presence of newly discovered lava flows of 36 Ma in the study area lying in the western MDVF indicates that volcanism was occurring at multiple locations within this area at 36 Ma, contradicting existing interpretations of age trends.

#### Inheritance and Rhyolite Petrogenesis

An ongoing controversy over the origin of large volumes of rhyolite ignimbrites erupted during the Cenozoic ignimbrite flare-up has to do with the relative contributions from differentiated mantlederived mafic magma sourced from subduction-modified sources (e.g., Farmer et al., 2008) and crustal melts (Rioux et al., 2016). In addition, there is uncertainty involving the magma generation process. Melting has been proposed to have occurred during subduction, following slab breakoff, or during post-subduction extension (e.g., Davis and Hawkesworth, 1994; McMillan et al., 2000; Szymanowski et al., 2019; Vermillion et al., 2024).

The hypothesis that felsic rocks in the Organ caldera formed from melts of the lower crust induced by mantle-derived basaltic magma was based primarily on isotope geochemistry (Rioux et al., 2016). We do not have isotopic data for this suite of rocks, but the abundant inheritance of Proterozoic zircons points to significant assimilation of crustal rocks.

Most samples contained inherited zircons. These fall into the following categories based on their likely sources: (1) ca. 1.6 Ga zircons derived from Mazatzal province gneisses or metasedimentary rocks (e.g., Amato et al., 2008), (2) ca. 1.5–1.4 Ga zircons derived from voluminous A-type granites in the region that directly underlie the Knight Peak volcanic sequence (e.g., Amato et al., 2011), (3) ages at ca. 1.2 Ga that are typical of the age of Grenville magmatism in the Burro Mountains about 25 km to the northwest (e.g., Rämö et al., 2003; Williams, 2015), and (4) three zircons ranging from 65–46 Ma, which could be related to the middle phase (63–55 Ma) of Laramide magmatism in the area (e.g., Amato et al., 2017).

Inheritance in the two samples of the C-Bar Canyon ignimbrite is quantified as consisting of 43 out of the 87 total analyses, or 49.4%. With approximately half of the zircons being derived from pre-existing crustal rocks, there are two possibilities: (1) the magma was derived at least in part from crustal rocks, as was postulated by Gonzales (2015) for plutons and dikes in southwestern Colorado, or (2) the xenocrystic zircons were derived from upper crustal rocks during eruption. If the latter hypothesis were likely, we would expect that the tuff breccia (sample 15BV-82) would have a higher proportion of inherited zircons than the sample with fewer lithics (sample 15BV-73). The lithic-poor sample had 64% inherited grains, whereas the lithic-rich sample had 41% inherited grains. Additional evidence that the inheritance occurred in the lower or middle crust, rather than the upper crust, is that a significant percentage of the inherited grains in the lithic-poor sample were from rocks with ages older than the 1.46 Ga granite exposed in the field area. The Mazatzal province ages range from 1.7 to 1.6 Ga and match known ages in the general area (e.g., Amato et al., 2008). Thus, we interpret the incorporation of older zircons in the rhyolite to have occurred during generation of the melt, and that at least part of the petrogenesis of this magma may have resulted from partial melting of the crust (e.g., Jacob et al., 2015).

# Tectonic Implications: Laramide and Basin and Range Deformation

We created two cross sections that interpret previous mapping (Figs. 2B and 3B). In the Pyramid Mountains (to the southwest of Knight Peak) and in the vicinity of Silver City (to the northeast), we observe that a Paleozoic sedimentary sequence up to 1000 m thick overlies basement and is itself unconformably overlain by a mid-Cretaceous marine sedimentary succession varying in thickness up to 100 m. These two sedimentary sequences were stripped off the Knight Peak structural block prior to deposition of the Paleogene volcanic rocks, or they were never deposited in the first place. Other workers have proposed that Paleozoic rocks were never deposited in the study area because of a local high during the Ancestral Rocky Mountains orogeny (e.g., Kues and Giles, 2004).

A restoration of the regional cross section (Fig. 2C) at the onset of MDVF and BHVF volcanism (~36 Ma) shows that the Knight Peak block was already a structural high. This high has been termed the "Burro Uplift" and interpreted to have formed as the result of Laramide deformation in the area (Mack and Clemons, 1988). Large-magnitude thrusts are exposed in the Chiricahua

Mountains of southeastern Arizona and have been interpreted to have been active between 60 and 35 Ma (Chapman et al., 2024). Similar inherited Laramide structures have been inferred to exist in the Silver City Range (Copeland et al., 2011); however, it is clear that the block tilting and regional structural grain of the Knight Peak area are due to Basin and Range deformation, and we suggest that the tilting of the volcanic rocks in the Silver City area may also be explained mainly by movement on post-Laramide Basin and Range normal faults.

We dated a representative rhyolite dike in the Knight Peak block at 59 Ma. This date is coeval with Laramide deformation in the region (e.g., Chapman et al., 2024). Numerous dikes of similar orientation and composition to the one we dated are exposed in the Knight Peak and Burro Peak blocks (Fig. 2A). The dominant orientation is 061 ± 15 (i.e., N61E; n=64; data compiled from the map of Drewes et al., 1985), and the dikes are most abundant adjacent to the Tyrone pluton in the Burro Peak block (unit TKg of Drewes et al., 1985). This suggests that the dikes are associated with the stock, and that the regional stress field had the most compressive stress oriented at about 060–240 (NE–SW) and the least compressive stress at about 150–320 (SE–NW). These values give an idea of the expected orientation of Laramide shortening of structures in the area.

On the western flank of Knight Peak, there is a small outcrop of Paleogene volcanic rocks that dip 15° to the northwest (Fig. 2A); therefore, the range is a broad anticline that we interpret as a rollover that developed on the hanging wall of the Knight Peak fault system. The cross-section restoration requires 5–10% extension during Basin and Range faulting.

Following the Malpais Hills lava flow at 32 Ma, there was a hiatus in volcanism before deposition of the Gila Conglomerate. The youngest volcanism in the MDVF and BHVF is around 24 Ma. The Gila Conglomerate has tilt-fanning dips that shallow systematically toward the Knight Peak fault (Fig. 3B). This unit is poorly dated but may be as old as early Miocene (Mack, 2004). These fanning dips provide geometric evidence for syntectonic sedimentation. We suggest that the structural data, combined with an apatite U/Th-He age of 19.9 ± 0.8 Ma from the Eagle Eye Peak block (also early Miocene: Gavel et al., 2021; average of n=5 grains from their table 1), provides strong evidence that the Gila Conglomerate deposition was coeval with displacement on the fault, exhumation of the Proterozoic rocks, and tilting of the volcanic units, and that all of these began in the early Miocene. However, our dates on volcanic rocks are slightly older than the onset of rapid exhumation based on multiple thermochronometers (Fig. 9; Gavel et al., 2021). It is possible that heating of the crust by the onset of voluminous magmatism in the MDVF and BHVF weakened the crust, causing large-scale extension and exhumation of basement blocks (e.g., Gans et al., 1989; Rosetti et al., 2017).

To summarize, the principal normal faults that control the regional structure are, for the most part, covered by Quaternary deposits. The Knight Peak normal fault is interpreted to dip around 45° to the southwest, and there is another parallel normal

fault <1 km to the southwest that is exposed north of the area shown in Figure 3A. We have projected this fault to the south where, despite being covered by younger deposits, it is required to keep the thickness of unit Tgc to <1000 m. Patches of Proterozoic granite (pCg) are exposed on the footwall block near the Knight Peak fault trace. In our interpretation, these two normal faults combined to have over 2 km of throw, and they are responsible for the steep tilt of the volcanic rocks (Fig. 3B).

#### **Conclusions**

The volcanic stratigraphy at Knight Peak was previously undated, with the exception of one sample originally misidentified as the Kneeling Nun Tuff. The study area lies at the southwestern edge of the MDVF and is near the most northeastern calderas of the BHVF; thus, the ignimbrites could have been sourced from calderas in either volcanic field, whereas the lava flows were sourced locally because most lava flows travel less than 50 km and typically significantly shorter distances than ignimbrites (e.g., Verolino et al., 2022).

There are four mapped volcanic units within this sequence, and the ages from these in order from lower to upper parts of the section are (1) JPB Mountain trachyte at  $36.2 \pm 0.6$  Ma; (2) C-Bar Canyon rhyolite breccia and tuff at  $35.2 \pm 0.4$  and  $35.2 \pm 0.6$  Ma, respectively; (3) KN78 rhyolite, dated by McIntosh et al. (1991), with a recalculated  $^{40}$ Ar/ $^{39}$ Ar date of  $34.0 \pm 0.2$  Ma; and (4) the Malpais Hills basaltic trachyandesite lava flow at  $32.6 \pm 0.4$  Ma. The JPB Mountain trachyte is the oldest unit in the western MDVF, and the only other units of this age are rhyolites from the Goodsight-Cedar Hills and the Organ Mountains in the eastern part of the province (Fig. 1; McIntosh et al., 1991; Zimmerer and

McIntosh, 2013). The new ages from this study can be used to suggest possible regional correlations that could be tested with additional high-precision geochronology and geochemistry.

Structural relationships combined with thermochronology indicate that there was a broad anticline formed from Paleozoic and Cretaceous sedimentary rocks during the Laramide orogeny, coeval with a rhyolite dike swarm at 59 Ma. Deposition of a thin, local conglomerate of unknown age was followed by the package of volcanic rocks (36–32 Ma) that experienced tilting by the Knight Peak fault and associated faults during Basin and Range extension, coeval with deposition of growth strata in the Gila Conglomerate and rapid cooling of the Knight Peak block based on apatite He data (Gavel et al., 2021) beginning in the early Miocene. The Basin and Range topography in the region results from movement on these faults. The majority of exhumation and cooling in the region may have slightly postdated the eruption of the volcanic rocks in this study.

## Acknowledgments

This work was done in partial fulfillment of the requirements of the Master of Science degree at New Mexico State University (NMSU) by the second author. Nancy McMillan helped acquire the XRF data at NMSU. The zircon ages were acquired at the Arizona LaserChron Center between 2016 and 2020, supported by EAR-1649254, with the help of George Gehrels, Mark Pecha, and Dominique Giesler. Karissa Vermillion and Jennifer Thines offered useful guidance on the manuscript. Discussions with Emily Johnson have always been informative. Reviewers Steven Cather, Matt Zimmerer, and editor Shari Kelley all provided useful input to improve the manuscript.

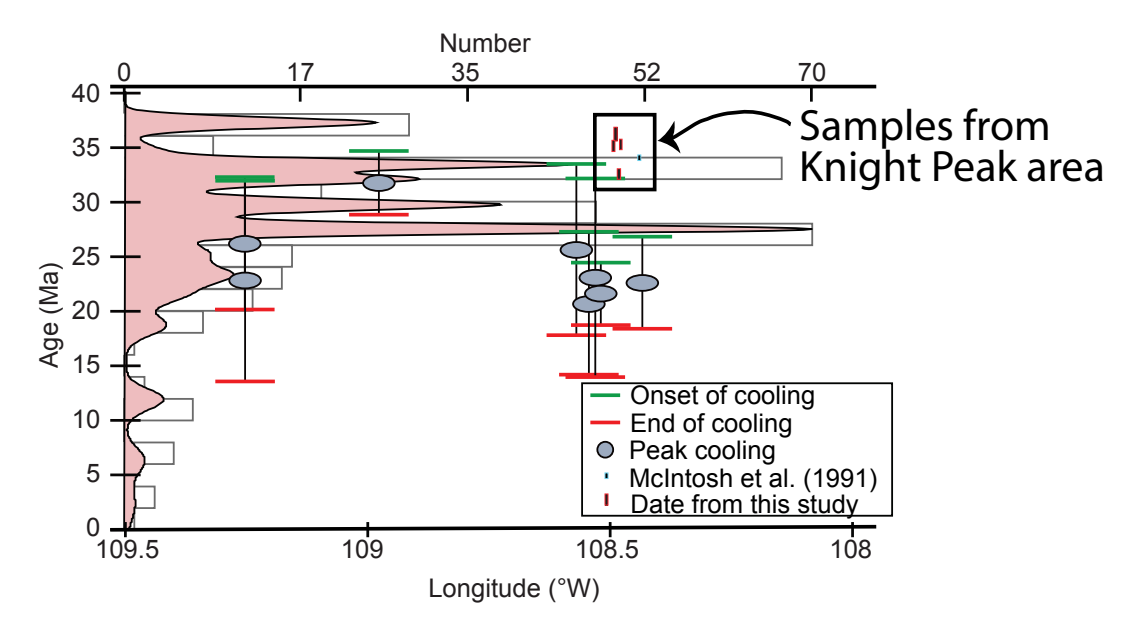


Figure 9. Kernel density estimation (KDE) curve (pink) for volcanism in the southeastern Basin and Range province and age histogram (n=317; data compiled from NAVDAT.org), as well as the onset (green bar), peak (gray oval), and end (red line) of cooling based on thermochronologic modeling, after Gavel et al. (2021). U-Pb zircon ages from this study in red and one <sup>40</sup>Ar/<sup>39</sup>Ar date from McIntosh et al. (1991) in blue. Volcanic rocks in this study appear to predate rapid cooling in southwestern New Mexico.

### References

- Amato, J.M., Boullion, A.O., Serna, A.M., Sanders, A.E., Farmer, G.L., Gehrels, G.E., and Wooden, J.L., 2008, Evolution of the Mazatzal province and the timing of the Mazatzal orogeny— Insights from U-Pb geochronology and geochemistry of igneous and metasedimentary rocks in southern New Mexico: Geological Society of America Bulletin, v. 120, no. 3–4, p. 328–346. https://doi.org/10.1130/B26200.1
- Amato, J.M., Heizler, M.T., Boullion, A.O., Sanders, A.E., Toro, J., McLemore, V.T., and Andronicos, C.L., 2011, Syntectonic 1.46 Ga magmatism and rapid cooling of a gneiss dome in the southern Mazatzal Province—Burro Mountains, New Mexico: Geological Society of America Bulletin, v. 123, no. 9–10, p. 1720–1744. https://doi.org/10.1130/B30337.1
- Amato, J.M., Mack, G.H., Jonell, T.N., Seager, W.R., and Upchurch, G.R., 2017, Onset of the Laramide orogeny and associated magmatism in southern New Mexico based on U-Pb geochronology: Geological Society of America Bulletin, v. 129, no. 9–10, p. 1209–1226. https://doi.org/10.1130/B31629.1
- Bachmann, O., and Bergantz, G.W., 2004, On the origin of crystal-poor rhyolites—Extracted from batholithic crystal mushes: Journal of Petrology, v. 45, no. 8, p. 1565–1582. https://doi.org/10.1093/petrology/egh019
- Ballmann, D.L., 1960, Geology of the Knight Peak area, Grant County, New Mexico: New Mexico Bureau of Mines and Mineral Resources Bulletin 70, 39 p. https://doi.org/10.58799/B-70
- Best, M.G., Christiansen, E.H., de Silva, S., and Lipman, P.W., 2016, Slab-rollback ignimbrite flareups in the southern Great Basin and other Cenozoic American arcs—A distinct style of arc volcanism: Geosphere, v. 12, no. 14, p. 1097–1135. https://doi.org/10.1130/GES01285.1
- Bhandari, S., Xiao, W., Ao, S., Windley, B.F., Zhu, R., Li, R., Wang, H.Y.C., and Esmaeili, R., 2019, Rifting of the northern margin of the Indian craton in the Early Cretaceous—Insight from the Aulis Trachyte of the Lesser Himalaya (Nepal): Lithosphere, v. 11, no. 5, p. 643–651. https://doi.org/10.1130/L1058.1
- Bornhorst, T.J., 1980, Major- and trace-element geochemistry and mineralogy of upper Eocene to Quaternary volcanic rocks of the Mogollon-Datil volcanic field, southwestern New Mexico [PhD thesis]: Albuquerque, University of New Mexico, 1104 p.
- Cameron, K.L., Nimz, G.J., Kuentz, D., Niemeyer, S., and Gunn, S., 1989, Southern Cordilleran basaltic andesite suite, southern Chihuahua, Mexico—A link between Tertiary continental arc and flood basalt magmatism in North America: Journal of Geophysical Research—Solid Earth, v. 94, no. B6, p. 7817–7840. https://doi.org/10.1029/JB094iB06p07817

- Castruccio, A., and Contreras, M.A., 2016, The influence of effusion rate and rheology on lava flow dynamics and morphology—A case study from the 1971 and 1988–1990 eruptions at Villarrica and Lonquimay volcanoes, Southern Andes of Chile: Journal of Volcanology and Geothermal Research, v. 27, p. 469–483. https://doi.org/10.1016/j.jvolgeores.2016.09.015
- Cather, S.M., Chamberlain, R.M., and Ratte, J.C., 1994, Tertiary stratigraphy and nomenclature for western New Mexico and eastern Arizona, *in* Chamberlin, R.M., Kues, B.S., Cather, S.M., Barker, J.M., and McIntosh, W.C., eds., Mogollon Slope (West-Central New Mexico and East-Central Arizona): New Mexico Geological Society Fall Field Conference Guidebook 45, p. 2 59–266: https://doi.org/10.56577/FFC-45
- Chapin, C.E., McIntosh, W.C., and Chamberlain, R.M., 2004, The late Eocene–Oligocene peak of Cenozoic volcanism in southwestern New Mexico, *in* Mack, G.H., and Giles, K.A., eds., The Geology of New Mexico—A geologic history: New Mexico Geological Society Special Publication 11, p. 271–293. https://doi.org/10.56577/SP-11
- Chapman, J.B., Clinkscales, C., Trzinski, A., and Daniel, M., 2024, Evidence for a Late Cretaceous to Paleogene basement-involved retroarc wedge in the southern U.S. Cordillera—A case study from the northern Chiricahua Mountains, Arizona: Geological Society of America Bulletin, v. 137, no. 3–4, p. 1827–1842. https://doi.org/10.1130/B37877.1
- Clemons, R.E., 1975, Petrology of the Bell Top Formation, *in* Seager, W.R., Clemons, R.E., and Callender, J.F., eds., Las Cruces Country: New Mexico Geological Society Fall Field Conference Guidebook 26, p. 123–130. https://doi.org/10.56577/FFC-26.123
- Coney, P.J., 1978, Mesozoic-Cenozoic Cordilleran plate tectonics, *in* Smith, R.B., and Eaton, G.P., eds., Cenozoic Tectonics and Regional Geophysics of the Western Cordillera: Geological Society of America Memoir 152, p. 33–50. https://doi.org/10.1130/MEM152-p33
- Coney, P.J., and Reynolds, S.J., 1977, Cordilleran Benioff zones: Nature, v. 270, p. 403–406. https://doi.org/10.1038/270403a0
- Copeland, P., Murphy, M.A., Dupré, W.R., and Lapen, T.J., 2011, Oligocene Laramide deformation in southern New Mexico and its implications for Farallon plate geodynamics: Geosphere, v. 7, no. 5, p. 1209–1219. https://doi.org/10.1130/GES00672.1
- Creitz, R.H., Hampton, B.A., Mack, G.H., and Amato, J.M., 2018, U-Pb geochronology of middle-late Eocene intermediate volcanic rocks of the Palm Park Formation and Orejon Andesite in south-central New Mexico, *in* Mack, G.H., Hampton, B.A., Ramos, F.C., Witcher, J.C., and Ulmer-Scholle, D.S., eds., Las Cruces Country III: New Mexico Geological Society Fall Field Conference Guidebook 69, p. 147–157. https://doi.org/10.56577/FFC-69.147

- Davis, J., and Hawkesworth, C.J., 1994, Early calc-alkaline magmatism in the Mogollon-Datil volcanic field, New Mexico, USA: Journal of the Geological Society, v. 151, no. 5, p. 825–823. https://doi.org/10.1144/gsjgs.151.5.0825
- Drewes, H., Houser, B.B., Hedlund, D.C., Richter, D.H., Thorman, C.H., and Finnell, T.L., 1985, Geologic map of the Silver City 1° x 2° quadrangle, New Mexico and Arizona: U.S. Geological Survey IMAP 1310-C, scale 1:250,000. https://doi.org/10.3133/i1310C
- Elston, W.E., Seager, W.R., and Clemons, R.E., 1975, Emory cauldron, Black Range, New Mexico—Source of the Kneeling Nun Tuff, *in* Seager, W.R., Clemons, R.R., and Callender, J.F., eds., Las Cruces Country: New Mexico Geological Society Fall Field Conference Guidebook 26, p. 283–292. https://doi.org/10.56577/FFC-26.283
- Erb, E.E., 1979, Petrologic and structural evolution of ash-flow tuff cauldrons and noncauldron-related volcanic rocks in the Animas and southern Peloncillo Mountains, Hidalgo County, New Mexico [PhD dissertation]: Albuquerque, University of New Mexico, 286 p.
- Farmer, G.L., Bailley, T., and Elkins-Tanton, L.T., 2008, Mantle source volumes and the origin of the mid-Tertiary ignimbrite flare-up in the southern Rocky Mountains, western U.S.: Lithos, v. 102, no. 1–2, p. 279–294. https://doi.org/10.1016/j.lithos.2007.08.014
- Gans, P.B., Mahood, G.A., and Schermer, E., 1989, Synextensional magmatism in the Basin and Range Province—A case study from the eastern Great Basin: Geological Society of America Special Paper 233, 53 p. https://doi.org/10.1130/SPE233
- Gavel, M.M., Amato, J.M., Ricketts, J.W., Kelley, S., Biddle, J.M., and Delfin, R.A., 2021, Thermochronological transect across the Basin and Range/Rio Grande rift transition—Contrasting cooling histories in contiguous extensional provinces: Geosphere, v. 17, no. 6, p. 1807–1839. https://doi.org/10.1130/GES02381.1
- Gaynor, S., 2013, Petrology, geochronology, geochemistry, deformation, and field relationships of the 1470–1450 Ma Burro Mountain intrusive suite [MS thesis]: Las Cruces, New Mexico State University, 162 p.
- Gonzales, D.A., 2015, New U/Pb zircon and <sup>40</sup>Ar/<sup>39</sup>Ar age constraints of the Cenozoic plutonic record, southwestern Colorado—Implications for regional magmatic-tectonic evolution: The Mountain Geologist, v. 52, no. 2, p. 5–42. http://dx.doi.org/10.31582/rmag.mg.52.2.5
- Gootee, B.F., Cook, J.P., Youberg, A., Douglass, J.C., Pearthree, P.A., and Heizler, M.T., 2021, Development and integration of the middle Gila River in the Safford basin, southeastern Arizona: Geomorphology, v. 399, 108074. https://doi.org/10.1016/j.geomorph.2021.108074
- Hedlund, D.C., 1978a, Geologic map of the Werney Hill quadrangle, Grant County, New Mexico: U.S. Geological Survey Miscellaneous Field Studies Map 1038, scale 1:24,000. https://doi.org/10.3133/mf1038

- Hedlund, D.C., 1978b, Geologic map of the C-Bar Ranch quadrangle, Grant County, New Mexico: U.S. Geological Survey Miscellaneous Field Studies Map 1039, scale 1:24,000. https://doi.org/10.3133/mf1039
- Hedlund, D.C., 1978c, Geologic map of the Burro Peak quadrangle, Grant County, New Mexico: U.S. Geological Survey Miscellaneous Field Studies Map 1040, scale 1:24,000. https://doi.org/10.3133/mf1040
- Hedlund, D.C., 1978d, Geologic map of the Gold Hill quadrangle, Grant County, New Mexico: U.S. Geological Survey Miscellaneous Field Studies Map 1035, scale 1:24,000. https://doi.org/10.3133/mf1035
- Hedlund, D.C., 1980, Geologic map of the Redrock SE quadrangle, Grant County, New Mexico: U.S. Geological Survey Miscellaneous Field Studies Map 1265, scale 1:24,000. https://doi.org/10.3133/mf1265
- Humphreys, E., Hessler, E., Dueker, K., Farmer, G.L., Erslev, E., and Atwater, T., 2003, How Laramide-age hydration of North America by the Farallon slab controlled subsequent activity in the western United States: International Geology Review, v. 45, no. 7, p. 575–595. https://doi.org/10.2747/0020-6814.45.7.575
- Jacob, K.H., Farmer, G.L., Buchwaldt, R., and Bowring, S.A., 2015, Deep crustal anatexis, magma mixing, and the generation of epizonal plutons in the Southern Rocky Mountains, Colorado: Contributions to Mineralogy and Petrology, v. 169, 7. https://doi.org/10.1007/s00410-014-1094-3
- Johnson, C.M., 1991, Large-scale crust formation and lithosphere modification beneath middle to late Cenozoic calderas and volcanic fields, western North America: Journal of Geophysical Research—Solid Earth, v. 96, no. B8, p. 13485–13507. https://doi.org/10.1029/91JB00304
- Kucks, R.P., Hill, P.L., and Heywood, C.E., 2001, New Mexico aeromagnetic and gravity maps and data—A web site for distribution of data: U.S. Geological Survey Open-File-Report 01-0061.
- Kues, B.S., and Giles, K.A., 2004, The late Paleozoic Ancestral Rocky Mountains system in New Mexico, *in* Mack, G.H., and Giles, K.A., eds., The Geology of New Mexico—A geologic history: New Mexico Geological Society Special Publication 11, p. 95–136. https://doi.org/10.56577/SP-11
- Kuiper, K.F., Deino, A., Hilgen, F.J., Krijgsman, W., Renne, P.R., and Wijbrans, J.R., 2008, Synchronizing rock clocks of Earth history: Science, v. 320, no. 5875, p. 500–504. https://doi.org/10.1126/science.1154339
- Lawton, T.F., Amato, J.M., Machin, S.E.K., Gilbert, J.C., and Lucas, S.G., 2020, Tectonic transition from Late Jurassic rifting to middle Cretaceous dynamic foreland, southwestern U.S. and northwestern Mexico: Geological Society of America Bulletin, v. 132, no. 11–12, p. 2489–2516. https://doi.org/10.1130/B35433.1
- Le Bas, M.J., Le Maitre, R.W., and Woolley, A.R., 1992, The construction of the Total Alkali-Silica chemical classification of volcanic rocks: Mineralogy and Petrology, v. 46, p. 1–22. https://doi.org/10.1007/BF01160698

- Mack, G.H., 2004, Middle and late Cenozoic crustal extension, sedimentation, and volcanism in the southern Rio Grande rift, Basin and Range, and southern transition zone of southwestern New Mexico, *in* Mack, G.H., and Giles, K.A., eds., The Geology of New Mexico—A geologic history: New Mexico Geological Society Special Publication 11, p. 389–406. https://doi.org/10.56577/SP-11
- Mack, G.H., and Clemons, R.E., 1988, Structural and stratigraphic evidence for the Laramide (early Tertiary) Burro uplift in southwestern New Mexico, *in* Mack, G.H., Lawton, T.F., and Lucas, S.G., eds., Cretaceous and Laramide Tectonic Evolution of Southwestern New Mexico: New Mexico Geological Society Fall Field Conference Guidebook 39, p. 59–66. https://doi.org/10.56577/FFC-39.59
- Mack, G.H., and Stout, D.M., 2005, Unconventional distribution of facies in a continental rift basin—The Pliocene–Pleistocene Mangas Basin, south-western New Mexico, USA: Sedimentology, v. 52, no. 6, p. 1187–1205. https://doi.org/10.1111/j.1365-3091.2005.00735.x
- McIntosh, W.C., and Bryan, C., 2000, Chronology and geochemistry of the Boot Heel volcanic field, New Mexico, *in* Lawton, T.F., McMillan, N.J., and McLemore, V.T., eds., Southwest Passage—A trip through the Phanerozoic: New Mexico Geological Society Fall Field Conference Guidebook 51, p. 157–174. https://doi.org/10.56577/FFC-51.157
- McIntosh, W.C., Kedzie, L.L., and Sutter, J.F., 1991, Paleomagnetism and <sup>40</sup>Ar/<sup>39</sup>Ar ages of ignimbrites, Mogollon-Datil volcanic field, southwestern New Mexico: New Mexico Bureau of Mines and Mineral Resources Bulletin 135, 99 p. https://doi.org/10.58799/B-135
- McIntosh, W.C., Chapin, C.E., Ratté, J.C., and Sutter, J.F., 1992, Time-stratigraphic framework for the Eocene–Oligocene Mogollon-Datil volcanic field, southwest New Mexico: Geological Society of America Bulletin, v. 104, no. 7, p. 851–871. https://doi.org/10.1130/0016-7606(1992)104%3C0851:TSF FTE%3E2.3.CO;2
- McMillan, N.J., 2004, Magmatic record of Laramide subduction and the transition to Tertiary extension—Upper Cretaceous through Eocene igneous rocks of New Mexico, *in* Mack, G.H., and Giles, K.A., eds., The Geology of New Mexico—A geologic history: New Mexico Geological Society Special Publication 11, p. 249–270. https://doi.org/10.56577/SP-11
- McMillan, N.J., Dickin, A.P., and Haag, D., 2000, Evolution of magma source regions in the Rio Grande rift, southern New Mexico: Geological Society of America Bulletin, v. 112, no. 10, p. 1582–1593. https://doi.org/10.1130/0016-7606(2000)112%3C1582:EOMSRI%3E2.0.CO;2
- Mizer, J.D., Barton, M.D., and Stegen, R., 2015, U-Pb geochronology of Laramide magmatism related to Cu-, Zn-, and Fe-mineralized systems, Central Mining District, New Mexico, *in* Pennell, W.M., and Garside, L.J., eds., Proceedings of the Geological Society of Nevada Symposium—New Concepts and Discoveries: Reno, Nevada, Geological Society of Nevada, v. 2, p. 1109–1129.

- New Mexico Bureau of Geology and Mineral Resources, 2003, Geologic map of New Mexico, scale 1:500,000. https://doi.org/10.58799/116894
- Pullen, A., Ibañez-Mejia, M., Gehrels, G.E., Giesler, D., and Pecha, M., 2018, Optimization of a laser ablation-single collector-inductively coupled plasma-mass spectrometer (Thermo Element 2) for accurate, precise, and efficient zircon U-Th-Pb geochronology: Geochemistry, Geophysics, Geosystems, v. 19, no. 10, p. 3689–3705. https://doi.org/10.1029/2018GC007889
- Rämö, O.T., McLemore, V.T., Hamilton, M.A., Kosunen, P.J., Heizler, M., and Haapala, I., 2003, Intermittent 1630–1220 Ma magmatism in central Mazatzal province—New geochronologic piercing points and some tectonic implications: Geology, v. 31, no. 4, p. 335–338. https://doi.org/10.1130/0091-7613(2003)031%3C0335:IMMIC M%3E2.0.CO;2
- Richard, S.M., Reynolds, S.J., Spencer, J.E., and Pearthree, P.A., 2002, Digital graphics files for the Geologic Map of Arizona, a representation of Arizona Geological Survey Map 35: Arizona Geological Survey DGM-17.
- Ricketts, J.W., Kelley, S.A., Karlstrom, K.E., Schmandt, B., Donahue, M.S., and van Wijk, J., 2016, Synchronous opening of the Rio Grande rift along its entire length at 25–10 Ma supported by apatite (U-Th)/He and fission-track thermochronology, and evaluation of possible driving mechanisms: Geological Society of America Bulletin, v. 128, no. 3–4, p. 397–424. https://doi.org/10.1130/B31223.1
- Rioux, M., Farmer, G.L., Bowring, S.A., Wooton, K.M., Amato, J.M., Coleman, D.S., and Verplanck, P.L., 2016, The link between volcanism and plutonism in epizonal magma systems; high-precision U–Pb zircon geochronology from the Organ Mountains caldera and batholith, New Mexico: Contributions to Mineralogy and Petrology, v. 171, 13. https://doi.org/10.1007/s00410-015-1208-6
- Rossetti, F., Asti, R., Faccenna, C., Gerdes, A., Lucci, F., and Theye, T., 2017, Magmatism and crustal extension—
  Constraining activation of the ductile shearing along the Gediz detachment, Menderes Massif (western Turkey): Lithos, v. 282–283, p. 145–162. https://doi.org/10.1016/j.lithos.2017.03.003
- Stegen, R.J., Barton, N.D., and Seedorff, E., 2024, U-Pb geochronology and major hydrothermal features of Laramide porphyry Cu-(Mo) deposits of southeastern Arizona and southwestern New Mexico, with a focus on Morenci, Safford, and Tyrone: Geological Society of America Abstracts with Programs, v. 56, no. 5. http://dx.doi.org/10.1130/abs/2024AM-402655
- Swenton, V.M., 2017, Using field relationships and geochronology to evaluate the formation of the Schoolhouse Mountain caldera, Mogollon-Datil volcanic field, southwest New Mexico [MS thesis]: Las Cruces, New Mexico State University, 199 p.

- Szymanowski, D., Ellis, B.S., Wotzlaw, J.F., and Bachmann, O., 2019, Maturation and rejuvenation of a silicic magma reservoir—High-resolution chronology of the Kneeling Nun Tuff: Earth and Planetary Science Letters, v. 510, p. 103–115. https://doi.org/10.1016/j.epsl.2019.01.007
- Vermeesch, P., 2018, IsoplotR—A free and open toolbox for geochronology: Geoscience Frontiers, v. 9, no. 5, p. 1479–1493. https://doi.org/10.1016/j.gsf.2018.04.001
- Vermillion, K.B., Johnson, E.R., Amato, J.M., Heizler, M.T., and Lente, J., 2024, Onset and tempo of ignimbrite flare-up volcanism in the eastern and central Mogollon-Datil volcanic field, southern New Mexico, USA: Geosphere, v. 20, no. 5, p. 1364–1389. https://doi.org/10.1130/GES02698.1
- Verolino, A., Jenkins, S.F., Sieh, K., Herrin, J.S., Schonwalder-Angel, D., Sihavong, V., and Oh, J.H., 2022, Assessing volcanic hazard and exposure to lava flows at remote volcanic fields—A case study from the Bolaven Volcanic Field, Laos: Journal of Applied Volcanology, v. 11, 6. https://doi.org/10.1186/s13617-022-00116-z
- Williams, W.A., 2015, Proterozoic sedimentation and magmatism in the Redrock area, Burro Mountains, southwest New Mexico [MS thesis]: Las Cruces, New Mexico State University, 146 p.
- Zheng, M., Song, Y., Li, H., Guilmette, C., Tang, J., Zhang, Q., Liu, Z., and Li, F., 2022, Triassic trachytic volcanism in the Bangong–Nujiang Ocean—Geochemical and geochronological constraints on a continental rifting event: Geological Magazine, v. 159, no. 4, p. 519–534. https://doi.org/10.1017/S0016756821001114
- Zimmerer, M.J., and McIntosh, W.C., 2013, Geochronologic evidence of upper-crustal in situ differentiation—Silicic magmatism at the Organ caldera complex, New Mexico: Geosphere, v. 9, no. 1, p. 155–169. https://doi.org/10.1130/GES00841.1